

# Chapter 6

## Shear Induced Nucleation

### 6.1 Introduction

One of the project aims is to investigate the possibility of using optical tweezing to induce nucleation by generating fluid flow within a supersaturated solution. The intent of which would be twofold: Firstly to have a repeatable means of inducing nucleation under different solution conditions. And secondly, to understand the influence of shearing on nucleation at a micro level as compared to results in bulk fluid.

It has been shown that for macro-scale systems, the likelihood of nucleation increases to a maximum value under increased shearing [1], [2]. Mura and Zaccone developed a theoretical framework to describe how the nucleation process when placed in a moving fluid, in which they highlighted two additional factors compared to a stationary fluid. Firstly, due to increased molecular transport of solute molecules the nucleation rate is enhanced in low to moderate fluid flows. But in addition, due to shear flow the crystal surface undergoes deformation which suppresses the nucleation rate undergoing faster fluid flow [2]. Experimental results with glycine solution support this theory; Debuyschere *et al* demonstrated that the nucleation rate of supersaturated glycine was enhanced up until  $\dot{\gamma} \approx 3000 \text{ } s^{-1}$  [1], after which the nucleation rate began to decrease but was still greater compared to the case where fluid flow was minimal.

Optical tweezers can been used to rotate a whole host of microscopic objects, with the fastest reported results exceeding 1000  $Hz$  in heavy water [3]. If such a micro-rotor

was suspended in a supersaturated solution the fluid flow around it could be fast enough that the nucleation rate is locally enhanced. We focused on two primary candidates for rotation, Vaterite and 4-Heptyl-4-biphenylcarbonitrile (7CB). The former being a polymorph of calcium carbonate and the latter an example of nematic liquid crystals, both of which have been used repeatedly in previous micro-rotor research [3]–[5]. In addition, we also consider the application of using techniques beam steering to generate fluid flow by trapping silica micro-beads. In this instance the fluid flow is generated not due to the transfer of angular momentum, but due to shearing caused by a moving sphere through stagnant fluid.

In this chapter we cover the basics of nucleation theory, in particular the development from the classical nucleation theory to the current non-classical theory. From there we discuss the experimental set up used during this project, highlighting some of the more notable optic techniques, before describing the synthesis and performance of different birefringent particles as optical rotors within supersaturated solutions. Lastly, we highlight some last minute results involving a galvano mirror and how the rapid movement of a optical trap can influence the growth and behaviour of a nucleus.

## 6.2 Nucleation

Nucleation is an example of a binary phase separation, where a dilute phase is miscible in a bulk phase, more often called the solute and solvent respectively. When a small amount of solute is added to the solvent the solute will diffuse throughout the solvent, reaching an equilibrium concentration throughout the solution. Because of molecular interactions, the two can only remain in equilibrium while below a specific concentration ( $C_{eq}$ ) - below which the chemical potential  $\mu$  for a single phase is greater than the potential required to separate the two. Once  $C_{eq}$  is exceeded there is a chemical potential difference driving the solution to separate the two phases. This does not mean that nucleation will occur immediately once  $C_{eq}$  is exceeded, only that there is a chemical potential supporting nucleation.

Since different combinations of solute and solvent will have different equilibrium con-

centrations, researchers often instead measure the ratio between the solute and solvent by using 'supersaturation' [6]:

$$S(T) = \frac{C_{sol}}{C_{eq}(T)} \quad (6.1)$$

Where  $C_{sol}$  is just the solute concentration, and  $C_{eq}(T)$  is the equilibrium concentration of the solute at temperature  $T$  based on the main solvent. While the solution remains supersaturated there is a chemical potential driving the solute to coalesce and separate from the solution as an ordered solid, the first formation of the crystal is referred to as the nucleus and understanding its formation has been the focus of researchers for decades now. Typically, for an industrial crystallisation process the working principle is based on controlling and manipulating the supersaturation of the system.

### 6.2.1 Primary & Secondary nucleation

nucleation process be broadly categorised into either primary or secondary nucleation. The former describes the formation of an initial nucleus within the bulk phase, absent of any external surfaces. Primary nucleation is dependent only on the local concentrations of the solute which can fluctuate unpredictably, as such it is often modelled at a large scale as a stochastic process. The only reliable factor being that higher supersaturations will result in more nucleation events to occur sooner.

An important metric for crystallisation procedures is the nucleation rate of the solution, a measure of the total volume or mass of crystalline material produced for a given set of initial conditions. At an industrial scale this metric is a contribution of both primary and secondary nucleation events. At a small scale one can estimate the contribution of the primary nucleation pathway by making repeated measurements of sample solutions and seeing how many have nucleated after a given time, giving us a Poisson probability distribution.

$$P(t) = 1 - \exp[-JV(t - t_g)] = \frac{M^*(t)}{M} \quad (6.2)$$

Where  $J$  is the nucleation rate,  $t_g$  is the 'growth time' which accounts for the

initial delay due to the stochastic nature of primary nucleation,  $V$  is the volume of the individual samples, and  $M^*(t)$  &  $M$  are the number of nucleated samples and the total number of samples used respectively. While (6.2) is useful for studying the effects of different parameters at a small scale, for industrial applications there are too many external factors for primary nucleation to be measured accurately. Overall while the primary nucleation rate is significant when studying solutions for small volumes, the contributions of secondary nucleation is far more significant when considering nucleation rate for an industrial crystalliser.

Secondary nucleation is the result of a initial seed crystal inducing further nucleation within the bulk solution [7]. The seed crystals are often prepared ahead of time and added to a supersaturate solution. Due to interactions with the surrounding fluid and the container walls it is possible for the seed crystals to act as a surface for further nucleation [8]. However this is just one possible way in which a seed crystal can enhance the nucleation rate, depending on the conditions of the crystalliser there are multiple mechanism by which the seed crystal can contribute to the nucleation rate of the system. Control of secondary nucleation events are crucial for ensuring reliable industrial crystalliser performance. Fig. 6.1 depicts an attempt of classifying every possible mechanism that could lead to secondary nucleation.

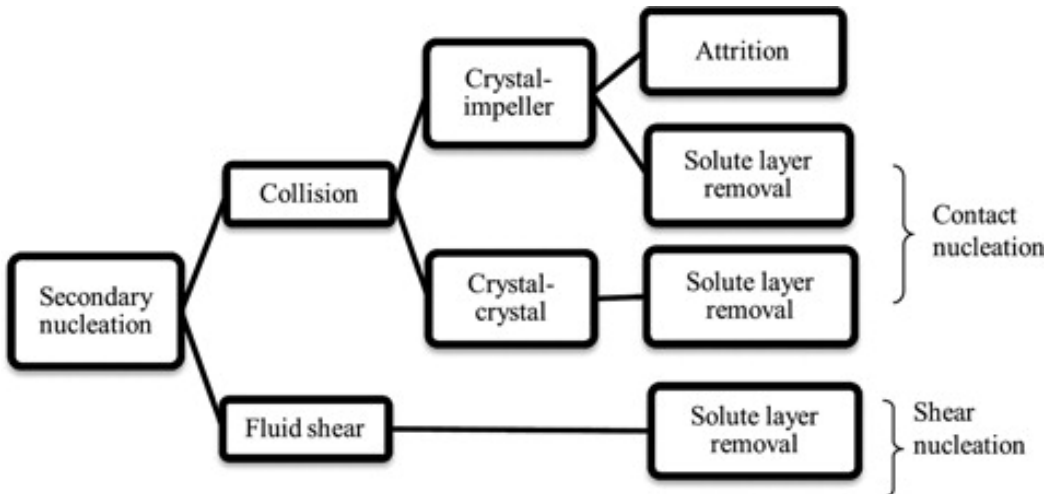


Figure 6.1: Secondary Nucleation mechanisms, classified by Agrawal and Paterson [9]

This is not a universal classification system, there are a variety of opinions on how

best to characterise different phenomena. It is heavily dependent on the theory used to describe nucleation events, this is accurate for both secondary and primary nucleation.

### 6.3 Nucleation Theories

In order to predict the nucleation rate of a given solution we need a solid understanding of how the individual molecules interact such that they transition from an unordered phase to a ordered phase. Over the years several theories have been proposed to explain how nucleation events occur, so far there has yet to be a standout candidate that reliably predicts the systems behaviour. Either they fail to accurately predict nucleation rates or more generally cannot describe new experimental results.

#### 6.3.1 Classical Nucleation Theory (CNT)

Sometimes referred to as 'Gibbs Nucleation Theory' the original theory was first formed from the works of Volmer and Weber, and Frenkel [10], [11]. While initially it was more focused on describing droplet formation in condensing vapours it was extrapolated to describe crystallisation. The central premise of classical theory is that nucleation occurs stochastically due to collisions between individual solute molecules, ions, or atoms. At the same time the bulk phase is resistant to the formation of a new phase. The competition between these random collisions and the bulk solution can be used to predict the probability of a newly formed nucleus.

Consider a supersaturated solution, at some time individual sub units collide rapidly, one after another, forming a nucleus of volume  $4\pi r^3/3$ . The newly formed phase has a lower chemical potential than the surrounding solution, reducing the free energy of the system. Simultaneously, the formation of a new interface is resisted by the bulk phase due to surface tension. The net free energy of the system for a nucleus of radius  $r$  is given as [12]:

$$\Delta G = \frac{-4\pi r^3}{3v} k_B T \ln(S) + 4\pi r^2 \sigma_{inf} \quad (6.3)$$

Where  $S$  is the supersaturation from eq. (6.1)  $v$  is the approximate volume of an

## Chapter 6. Shear Induced Nucleation

individual molecule,  $k_B$  is the Boltzmann constant, and  $\sigma_{inf}$  is the interfacial tension of the bulk solution. This assumes that the nucleus will have a spherical morphology so that the surface tension  $\sigma_{inf}$  is a scalar value. Looking at (6.3) suggests that there must be some critical size  $r$  where the free energy gain from the nucleus exceeds the surface tension of the surrounding fluid. This is reflected in fig. 6.2 where we plot the free energy of the system against nucleus size. This reveals a critical size above which the gain in free energy exceeds the interfacial tension. Furthermore fig. 6.2 shows how increasing the supersaturation of the system reduces said barrier.

The maximum value of  $\Delta G_{tot}$  is the free energy barrier that any newly formed nucleus needs to overcome in order to stabilise. The nucleation rate (the volume of new crystalline material formed per unit time), is therefore commonly defined as being dependent on the energy barrier  $\Delta G^*$ :

$$J = A \exp \left[ -\frac{\Delta G^*}{k_B T} \right] \quad (6.4)$$

Where  $A$  is a pre-factor that can be fine tuned to the exact demands of the system, the free energy barrier can be found by finding the stationary point of  $\Delta G_{tot}$ .

CNT is often regarded as a good description of the macro system, its obvious that for all crystallization systems there is an inherent energy barrier that must be overcome prior to nucleation. Where it falters is in its predictive ability, both in estimating nucleation rates [13], [14], and in the structure of newly formed nuclei [15], [16]. Recent studies suggest classical nucleation is merely one of many possible pathways that can be taken to produce an ordered crystalline phase. In situations where the solution is heavily saturated with solute the driving force promoting nucleation is so large that a nucleus can form in the bulk solution in a single step.

This is however not accurate at lower supersaturations, closer to the saturation point the solvent's surface tension is so significant that the addition of individual solute molecules should not be enough to overcome the dissolution of the nucleus. And yet nucleation is still possible, occurring far more reliably than predicted by the CNT. This suggests that the formation of a nucleus is due to larger aggregates of solute that are

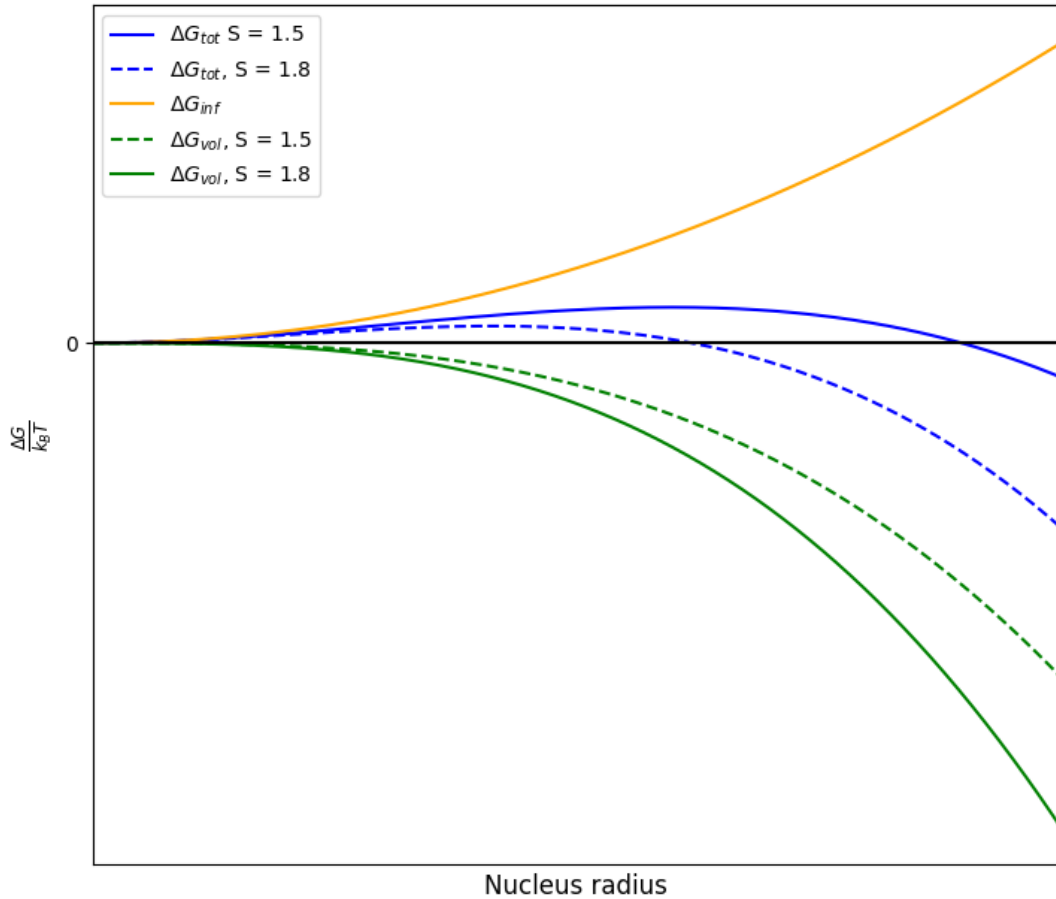


Figure 6.2: Free energy diagram of a newly formed nucleus according to the Classical Nucleation Theory. The total free energy (blue) is due to the competition between the volume free energy gain (green) and the interfacial free energy cost (orange). Dotted lines are for a higher supersaturation than the solid lines, the interfacial energy cost is independent of supersaturation. Diagram was constructed in python using a naive assumption of  $v = 1 \times 10^{-12} m^3$  and  $\sigma_{inf} = 0.0001 J/m^2$

stable within the bulk solution. This has been confirmed experimentally and lead to the development of Two Step Nucleation.

### 6.3.2 Two Step Nucleation

The two step nucleation theory is an extension to the CNT that suggests that prior to nucleation, the solute will form precursor structures. The CNT assumes that solute structures below the critical radius should be unstable within the solution due to in-

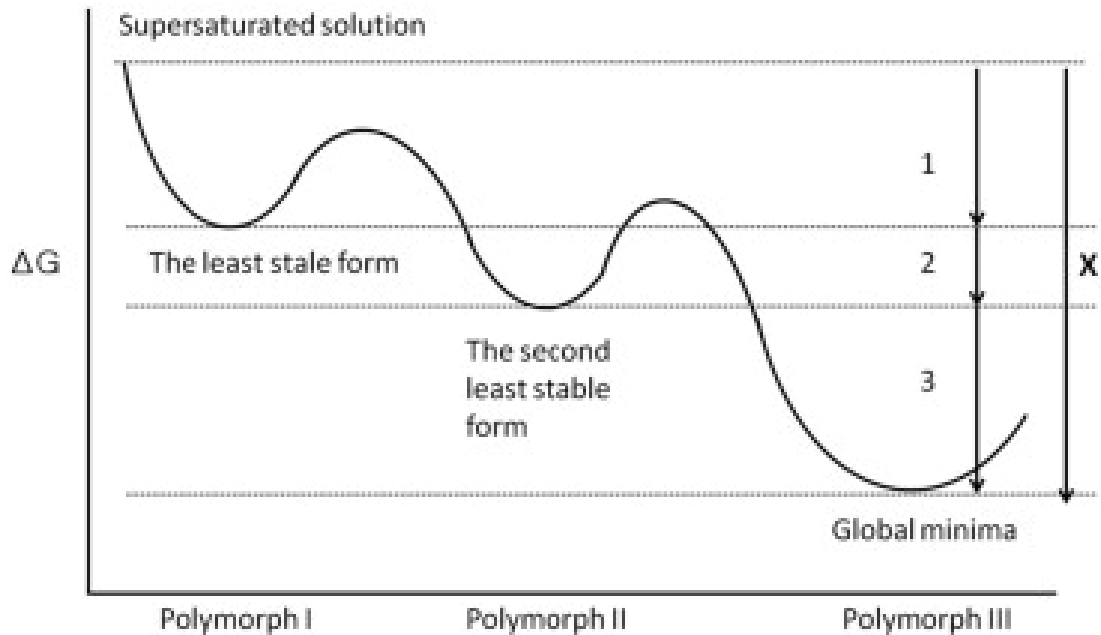


Figure 6.3: Free energy diagram of Oswald's rule for a crystal with three possible polymorphs. The diagram shows that there exist local minima in the free energy that represent the different polymorphic forms. A similar free energy diagram can be used to describe the two-step nucleation mechanism.

terfacial forces trying to dissolve the solute. This assumption is based on the idea that any interactions between solute molecules are much weaker than that between solute and solvent molecules. If instead the solute molecule interactions are significant then it stands to reason that subcritical liquid-like structures are stable.

The first observation of a liquid-like structure was in  $CaCO_3$  solutions, initially it was assumed that polymers were a necessary additive to create a precursor structure [12], [17]. This is not the case when the solution is above its critical temperature, allowing the solution to be in the binodal region of the phase diagram. This would result in the formation of two liquid phases, one being rich in solute, the other being solute poor [12], [18]. Several papers later reported the presence of stable liquid-like clusters that formed prior to nucleation [19]–[21].

The formation of these clusters can be understood by Oswald's rule; which says that any crystallising system does not immediately take the path to the lowest possible energy state but instead first transitions to the state with the smallest free energy

barrier [22]. Oswald's rule was assumed to be applicable for crystal polymorphs but can be generalised to describe the nucleation process also. Further phase transitions can still occur but the pathway taken should always minimises the overall free energy cost. It is assumed that between the amorphous phase and the crystalline phase the solute undergoes dehydration while changing structurally into a more ordered phase, though there is some discussion whether the process merely undergoes dehydration, or if there is a more complex chemical reaction [12].

With regards to liquid-precursors, there is still a lot of discussion about the relationship between the solution conditions and the the precursors. The size and rate at which these precursors agglomerate based on the degree of saturation would provide invaluable information on the kinetics of two-step nucleation [18]. In some cases it has even been shown that 'ageing' solutions is a necessary step in order to detect the presence of stable amorphous clusters [23]. This was in solutions that were supersaturated and yet after the formation of precursors spontaneous nucleation was not seen even after several days of observation [23]. This suggests that in some cases the precursors are metastable and require an external trigger to induce crystallisation. The presence of metastable structures and other phenomena has lead to development of a more universal theory, namely non-classical nucleation.

### 6.3.3 Non-classical Nucleation

Two-step nucleation is based on the idea that between the bulk solution and the final crystalline phase there exists and intermediate stage. While this is broadly an accepted concept, research has shown that in some cases the intermediate stage can be subdivided into multiple states. This has been shown to be the case with metals in both solid and liquid conditions [24], [25] and colloidal simulations have indicated that the precursors undergo structural change over time [26]. While in some cases it has been possible to directly monitor the structural change in the amorphous clusters, many organic compounds have not received such treatment due to the difficulty of characterising and monitoring the pre nucleation stage [18]. This is often why two-step nucleation is simply referred to as multi-step nucleation.

There are also a myriad of other unique nucleation events that deviate significantly from both the classical and two-step nucleation theories. A review paper discussing recent advances in non-classical crystallisation highlighted that depending on the collision kinetics of the system and the molecular interactions could result in drastically different reaction kinetics. In the former case, unstable subcritical nuclei have been shown to collide and coalesce into a supercritical nucleus, but only in conditions where subcritical nucleation are plentiful despite a low degree of supersaturation [27]. The latter case is more prevalent for dipole solute molecules, the anisotropic attraction results in nuclei with non-spherical geometries, this results in varying kinetics for agglomeration dependent on the orientation of each molecule [16]. Phenomena such as the above examples has been collectively refereed to as non classical nucleation, it is known that they must be related to both CNT and multi-step nucleation but the connection is not clear based on the current literature.

As such, much of the research into nucleation theory is focused on developing *in situ* techniques that can monitor and characterise the pre nucleation stage, this would glean information on cases when both classical and non-classical nucleation is a possibility [12].

## 6.4 In situ techniques for studying nucleation

There are several different phenomena [12], [18] that are not well described by any individual theoretical framework (CNT or multi-step nucleation for example). There is an increasing interest in probing the pre-nucleated solution.

One of the key conclusions is the need for the development of better *in situ* techniques for characterizing and imaging the nucleation pathways. Understanding which specific pathway is unfolding under a certain set of experimental parameters would allow one to develop a map of the thermodynamic landscape available to a pre-nucleation system. The challenge therein lies in developing experimental methods by which one can reproduce similar nucleation events and in turn use characterisation techniques to identify the pathway taken. The method not only needs to be repeatable for a single set

of system parameters, but also needs to be flexible enough to replicate results regardless of the system parameters (i.e. varying supersaturation, temperature, and solute choice). There have been several different methods deployed to try and observe crystallisation at a microscopic scale.

#### 6.4.1 Computer Simulations

While not a direct observation of nucleation events, computer simulations have proved an invaluable tool for studying and testing predictions about the pre-nucleated solution. By comparing the simulative nucleation rate to the expected rate given by current models, researchers can test newly developed theories and glean information about the microscopic parameters of a system.

The main challenge facing computer simulations is the issue of limited scope. Molecular dynamic simulations are constrained by their choice of time and length scale, for example simulations in a canonical ensemble face issues where the chemical potential is depleted to the point that the driving force for crystallisation is halted [28], [29], this can be addressed but requires an extensive increase in computational resources to maintain the chemical potential equilibria. Likewise in most cases the choice of time scale is a crucial factor, shorter time scales provide a more accurate evolution of the solution; however, in some cases the time scale magnitude for crystallisation is often far greater than the time scale used in the simulation. This has led to more advanced sampling techniques that allow for longer time scales which has provided insights into the pre-nucleation solution stage and formation of pre-nucleated clusters [29].

The study of the pre-nucleated solution and the evolution of precursors has been aided greatly by the use of simulative studies. Early on it was shown in colloidal crystallisation that the structure of the precursor was time dependent; colloidal simulations showed that regardless of the molecular interactions between colloids the atomic packing pattern was predominately hexagonal centred, over time the packing became dominated by body centred packing in the case where the interactions were longer reaching [26]. They also confirmed that precursor formation was driven not by local density variations, but instead was driven by the local bond order of the colloidal precursors [26], providing

strong evidence that the colloidal pre-nucleation clusters undergo rearrangement prior to nucleation. Further developments in *NaCl* simulations have shown that by varying the density fluctuations the precursor structure could either be amorphous, the classical rock-salt structure, or a new structure similar to wurtzite. While this result is difficult to confirm it provides an important conclusion, that simulations can hint at new nucleation pathways that have not been confirmed experimentally. This means that computer simulations can not be merely used to confirm theories, but can be used to examine and search for novel results.

Overall computer simulations make up a core area of research in the study of nucleation. The technique is however limited, often struggling to examine nucleation over longer time scales or larger number of particles. While sampling methods and enhanced simulation techniques have alleviated this somewhat they are still far from being able to describe the behaviour of larger molecules undergoing nucleation.

#### 6.4.2 Transmission Electron Microscope (TEM)

One of the more well known techniques used for direct observations of crystallisation dynamics is using transmission electron microscopy (TEM). The basic working principle involves creating a focused beam of electrons that are directed onto a target sample. Due to the wave-particle duality, the electrons can be treated as a unified beam of light, whose wavelength is dependent on the kinetic energy of the electrons. The wavelength of an individual electron is given by [30]:

$$\lambda_e = \frac{h}{\sqrt{2mE(1 + \frac{E}{2mc^2})}} \quad (6.5)$$

When incident on a sample the wave is scattered by the sample and can then be detected by an imaging screen that measures the difference in intensity between the scattered and transmitted beams. The advantage of TEM is that one can bypass the diffraction limit imposed by visible light, the maximum resolution that can be achieved by a microscope

is given by [31]:

$$d = \frac{\lambda}{2NA} \quad (6.6)$$

where NA is the numerical aperture of the objective lens, and  $\lambda$  is the wavelength of light used to illuminate a sample. For a visible light LED with an average wavelength of  $550\text{ nm}$ , the upper limit for an objective lens (NA of 1.2) is around  $230\text{ nm}$  whereas a similar lens focusing an electron beam with an average kinetic energy of  $100\text{ keV}$  will have a maximum resolution of just over  $4\text{ pm}$  [31]. There is an upper limit to the maximum resolution possible as electron lenses are far inferior to what modern optics can achieve [31] so there is a trade off between quality and resolution.

TEM technology has proven invaluable to the study of nucleation at an atomic level. The samples are often only a few hundred atoms thick in order to optimise the imaging results. Much of the supporting evidence for non-classical nucleation has been demonstrated via TEM [25]. For example when Cao *et al* observed the formation of amorphous atomic cluster using  $\gamma$ -Fe, Au, and Re; all three of which underwent continuous transformation before eventually reaching a final ordered state [24]. The amorphous cluster did not immediately transition to an ordered structure, instead fluctuating somewhat randomly until eventually settling into a crystalline structure [24]. This was confirmed both in solid growth and liquid growth conditions [24], [32], suggesting that the non-classical nucleation path dominates in all cases of metal crystal formation [25]. Confirmation is necessary for different solute choices, as in the case of organic solids it is believed that non-classical nucleation only dominates in low supersaturations whereas classical nucleation is dominate at higher supersaturations.

TEM analysis has not been extended to the study of organic crystals, proteins, or simple salts at an atomic level however. The main reason being that organic materials can be damaged by the electron beam and therefore need to be frozen prior to being imaged [31]. This was used to study the polymorphic time dependence of glycine crystals, by varying the time prior to freezing Broadhurst *et al* showed that  $\beta$  glycine dominates initially but  $\alpha$ - glycine is more stable after a longer period,  $\gamma$ -glycine was

only found when allowed to dry over an hour on a glass slide [33]. While this was invaluable for showing the time scales with which polymorphs form, it doesn't provide much information on the kinetics of crystal growth as these were snap shots and not direct observations of the nucleation process.

Overall TEM analysis is invaluable for the study of atomic crystal growth, the secondary scattering from electron beams also allows for chemical and structural information to be gleaned from the target. This has given strong evidence for the non-classical nucleation theory, particularly in metal crystal formation. Due to the high energy of the electrons, organic materials have not received the same focus outside of cryoTEM analysis. Non-invasive methods are therefore necessary to gain an understanding of the crystal growth and formation of organic crystals, particularly when both classical and multi-step nucleation can occur.

## 6.5 Optical Tweezer Equipment

In general, all optical tweezers require a laser driver, a focusing microscope objectives, a position controller, and position detector [34]. The laser used for this project was a 1064 nm near infrared laser - provided by CNI Lasers – that was focused by a Nikon 100x oil immersion lens. The choice of an oil immersion lens is important as the optical oil used prevents a loss of focus when used on a glass cover slip. Now, experimental work has shown that the trapping efficiency increases with beam diameter up until it exceeds  $\frac{2}{3}D_{obj}$  [35] where  $D_{obj}$  is the diameter of the objective aperture. To expand the beam front we utilise a Galilean beam expansion arrangement (indicated by  $f_1$ , and  $f_2$  in Fig. 6.4) as recommended for high power laser applications. In our initial experiments the beam expansion provides a 4 $\times$  magnification. Whereas in later experiments we utilised a galvano-mirror the beam expansion is 3 $\times$  and then the 4f correlator (see 6.5.2) provides a further 1.25 $\times$  magnification (using  $f_3$  and  $f_4$ ) - the magnification is given by.

$$\frac{D_2}{D_1} = \frac{f_2}{f_1} \quad (6.7)$$

It should be noted that the galvano-mirror requires the use of a Keplerian beam expansion arrangement which reduces the transmitted laser power due to localised heating of the air. Afterwards the laser is passed through a dichroic mirror that separates incoming infrared and visible light, this is to prevent the laser from damaging the CCD camera used for imaging the trapping plane. The laser is then focused to a diffraction limited spot by the objective. Utilizing a high numerical aperture objective enhances the gradient force at the focal point; the trade-off being that for higher NA objectives the trapping depth is reduced due to spherical aberrations. While it is possible to increase the trapping depth [36] by adjusting the objective's tube length this approach is incompatible with our trapping arrangement. A 0.25 NA condenser objective refocuses the scattered laser light and also provide an aperture for an imaging LED to illuminate the focal plane. Samples are loaded onto a piezo driven table to that is inserted between the trapping and condensing objectives; the piezo drivers allow for sub-micron control of the beam focus position to a degree as small as a 10 nm. To detect and monitor the position of a trapped particle a quadrant photo diode (QPD) was utilised.

In order to rotate birefringent particles a quarter-wave plate was installed via a rotating optic after  $f_4$  (the exact placement in the is not specific). When the quarter wave plate's is aligned with the electric field of the laser we have linearly polarised light, and when rotated by 45 deg the laser is now circularly polarised. Finding the point where the wave plate aligns with the laser was achieved by measuring the power output and finding its maximum. When a birefringent particle is trapped and the quarter wave plate is adjusted the particle will begin to rotate - assuming the fluid drag torque is less than the optical torque.

### 6.5.1 Galvano-Mirror

Later on in this chapter we discuss the impact of a moving beam front on the growth behaviour of a nucleating system. In order to do so we need a means of rapidly displacing the beam focus, for our purposes we chose a galvano-mirror. Galvano-mirror's are a method of beam steering, using a set of motorised mirror mounts the laser can be moved rapidly in any number of regular patterns.

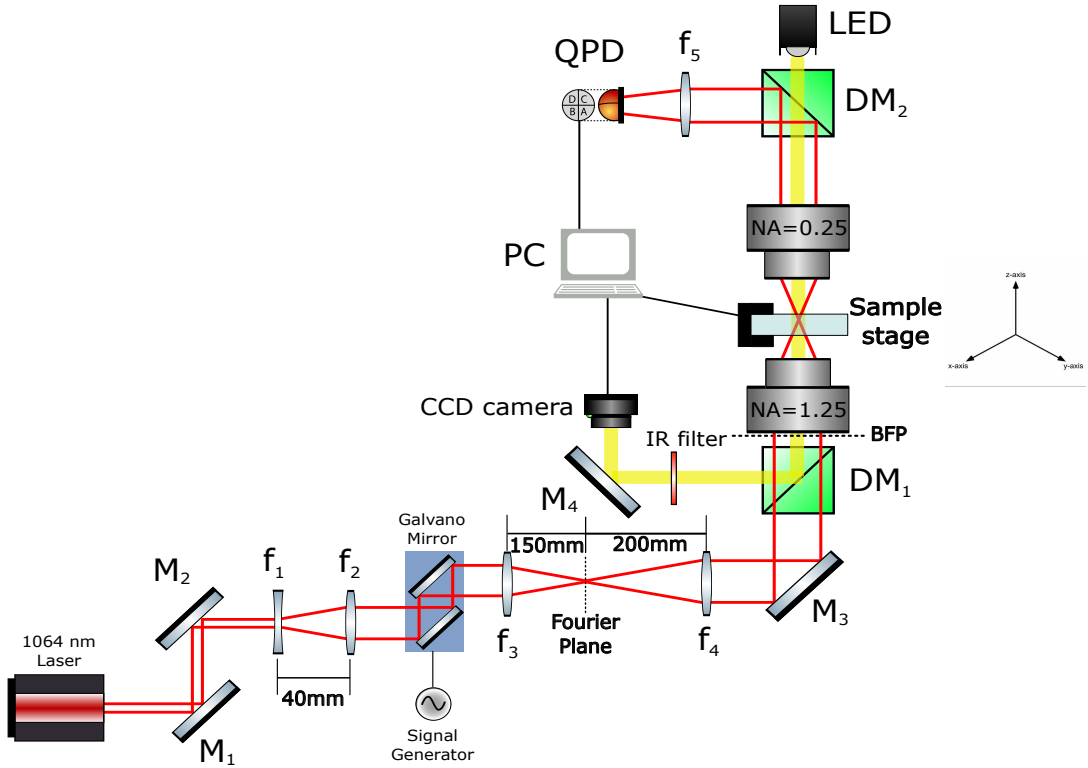


Figure 6.4: Optical tweezer set up used for the majority of the work. The focal lengths are  $f_1 = -20\text{ mm}$ ,  $f_2 = 60\text{ mm}$ ,  $f_3 = 150\text{ mm}$ , &  $f_4 = 200\text{ mm}$  [M = mirrors, DM = dichroic mirrors, f = focal lenses]. Diagram not drawn to scale.

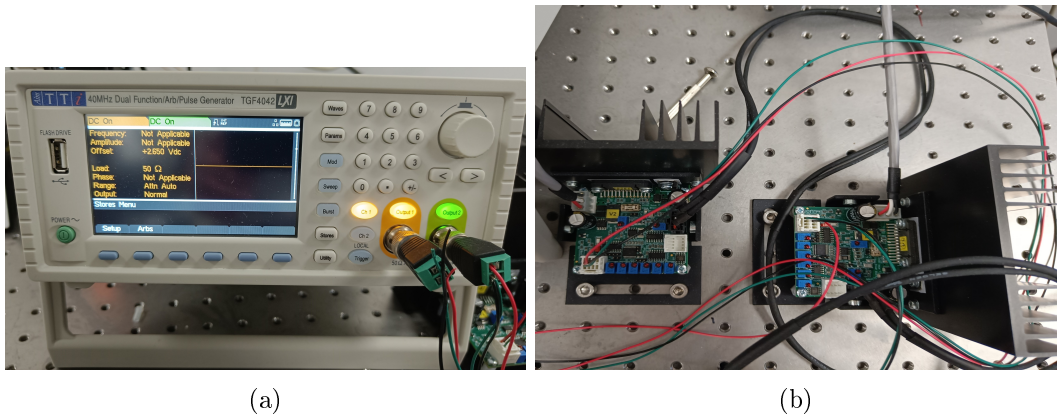


Figure 6.5: Signal generator galvo mirror controller, channel 1 controls the  $x$ -axis mirror, while channel 2 controls the  $y$ -axis mirror. Both channels can be manipulated independently.

The signal generator used was supplied by 'MCS Test Equipment Ltd', allowing for dual channel signal control. This allowed us to precisely control the amplitude, phase,

and frequency of both mirrors making alignment much easier.

While in theory the frequency can be increased until the mechanical limit of the mirrors is reached ( $\approx 1000\ Hz$ ), the practical upper limit is determined by the trap strength. For a silica sphere this is on the order of  $300\ Hz$  when suspended in water. Likewise while in theory the signal amplitude can be increased until the voltage limit of the motors is reached ( $\approx 5.0V$ ) the geometry of the focal lenses limits the maximum amplitude to  $0.5V$  as any greater will move the laser beyond the lens. For basic trapping calibration the galvano-mirrors were set to DC output, providing a fixed spot which operates like a typical optical trap.

### 6.5.2 Fourier Optics and 4f correlators

As shown in 6.4, after the galvano-mirror there are a pair of focal lenses ( $f_3$  and  $f_4$ ) that do not seem to serve a clear purpose. These are in fact crucial for the operation of the Galvano, the pair of them can be more accurately called a 4f correlator.

A 4f correlator is an example of Fourier optics in practice, understanding that a focused lens takes a Fourier transform of the light profile. Consider a laser with a circular Gaussian profile, if you were to place a detector there you would pick up the intensity as a function of its position within the beam. If however you focused the light into a single point (using a +ve focal lens) you are actually seeing a measurement of the phase of your laser with position, in which you would see a diffraction limited spot, indicating that the laser is collimated. In imaging systems, a series of focal lenses can be used to filter out unwanted scattering from an image (or in an inverse case differentiate between different images), the placement of each lens is shown in Fig. 6.4.

For our applications a 4f correlator is utilised to ensure that the motion of the galvano-mirrors does not move the focal point of the laser, allowing for a stable trap even while in motion. As shown in Fig. 6.4, after the galvano-mirror we have our two lenses -  $f_3$  and  $f_4$  - the former being installed  $150\ mm$  from the second mirror of the galvano, and the latter being installed  $200\ mm$  from the back focal plane of the trapping objective.

## 6.6 Synthesis of Birefringent Micro-spheres

There are several options for particles that can be rotated using optical tweezers [4], [5]. Over the course of the project two different micro spheres where investigated, Vaterite and liquid crystal droplets. Both can be readily synthesised in the lab and are will rotate at a variety of sizes (see ??).

Vaterite is a polymorph of calcium carbonate that is rarely seen in nature due to its low stability [37]. All three polymorphs are inherently birefringent meaning that they can be rotated using circularly polarised light. However unlike its other polymorphs of calcite and aragonite, when synthesised vaterite will typically form small spherical particles making them ideal for optical trapping and rotation. Synthesis of Vaterite micro spheres requires fine control of the crystal growth process in order to maintain polymorphic stability. Though for the purposes of optical rotation the exact polymorph is not as important as the morphology as all 3 polymorphs are inherently birefringent.

Vaterite samples where made by the first preparing equal amounts of  $CaCl_2$  and  $Na_2CO_3$  at a concentration of  $0.33M$ , at the same time a vial of  $0.33M$   $MgSO_4$  was prepared and set aside for later. First a small vial was filled with  $1.5mL$  of  $CaCl_2$  followed by  $60\mu L$  and  $90\mu L$  of  $MgSO_4$  and  $NaCO_3$  respectively, forming a seed solution. Next, a larger vial was filled with  $5\text{ mL}$ ,  $1.5\text{ mL}$ , and  $1\text{ mL}$  of  $CaCl_2$ ,  $MgSO_4$ , and  $NaCO_3$  respectively followed by the seed solution. After 10 minutes of slow but continuous mixing a few drops of Agepon was added to halt the reaction, the solution was filtered and washed 3 times with distilled water before being suspended in water.

When trapped in circularly polarised light, the anisotropic crystal lattice allows spin angular momentum to be transferred to the Vaterite particle, resulting in a rotation about the beam axis. Because the particle scatters light anisotropically the signal detected by the QPD shows periodic fluctuations [38]. In addition due to the change in polarisation there is also a periodic variation that appears at twice the rotational frequency [39]. Therefore, the resulting power spectrum is not a Lorentzian but now also displays peaks that appear at integer multiples of the particles rotational frequency.

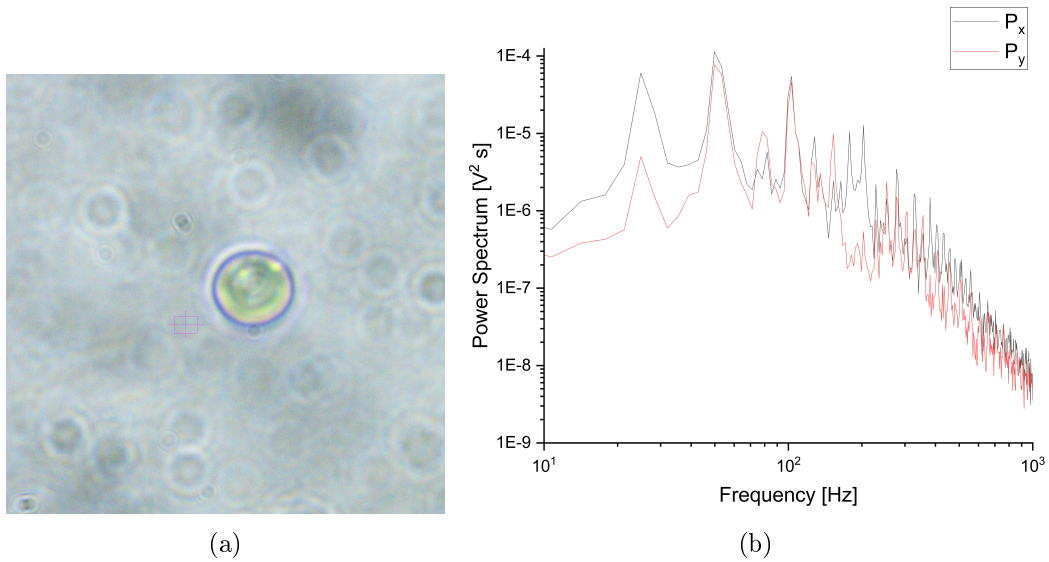


Figure 6.6: (a) Vaterite sphere suspended in water and trapped by circular polarised trap. (b) Collected power spectrum from rotating Vaterite, peaks in the power spectrum appear at integer multiples of the rotational frequency ( $f_{rot} \approx 49.8$  Hz)

As shown by Fig. 6.6(b) the power spectra produced still demonstrates a Lorentzian curve but modified with these periodic peaks, while the Lorentzian can be loosely fitted to the end tail there exists no current model for describing the power spectra. The closest approximation to this was conducted by [38] where they describe the rotational motion of ellipsoidal polystyrene particles. The critical assumption being that the particle perfectly rotates in the  $x - y$  plane. It has long been suspected that birefringent microspheres experience torques outside of the  $x - y$  plane [40] making it very difficult to characterise the behaviour of rotating birefringent microspheres without a proper understanding of the full optical torque being applied to it.

### 6.6.1 Liquid Crystal Rotors

Liquid crystals are an intriguing example of materials with mixed phase properties. Unlike typical solutes such as Glycine, a liquid crystal can still maintain some degree of order between its individual molecules while in the liquid state. This is due to the fact that liquid crystals are constructed of ordered molecules that demonstrate a long range ordering. There are three main types of liquid crystal transition methods: Ther-

## Chapter 6. Shear Induced Nucleation

motropic crystals will transition to their liquid crystal phase when sufficiently heated. Lyotropic materials can undergo this transition due to changes in temperature and concentration. And lastly, Metallotropic materials - which are composed of both organic and inorganic molecules - change phase according to the ratio of organic to inorganic molecules present. Liquid crystal rotors are rather simple in their production, 4-Heptyl-4-biphenylcarbonitrile (7CB) was purchased from Sigma Aldrich and a small amount was added to a vial of distilled water. The solution was then heated in a water bath to 25° in order to transition the solid crystal into its liquid crystal state. The solution can then be loaded onto a sample cover slip and the individual droplets visualised. The molecules of 7CB will align with a strong electric field, and due to the spherical droplet geometry the droplets are inherently birefringent.

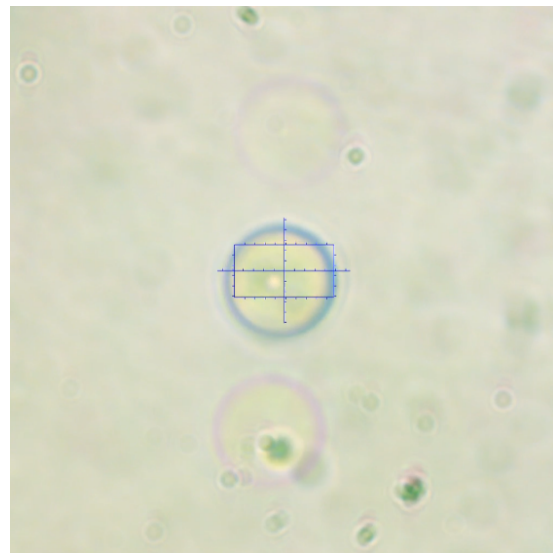


Figure 6.7: Liquid crystal undergoing rotation due to the circularly polarised trap.

The liquid crystal droplets had a much faster rotation rate than comparable Vaterite spheres, due to their higher degree of birefringence and the fact that the droplets are far closer to perfect spheres making angular momentum transfer more efficient.

## 6.7 Rotation of birefringent micro spheres

Optical tweezing has often been used for micro-rheology, by computing the exact forces being exerted on the trapped sphere, one can determine the local temperature/viscosity of the medium [41], [42].

When it comes to optical rotation, a rotating particle will experience a fluid drag torque that is proportional to its rotation rate, the maximum rotation rate is when the fluid drag is equal to the optical torque of the laser [42]. Optical rotors have been used to measure local temperature changes [41], or for understanding how fluid shear propagates through a medium [43]. Likewise, one can use a beam steering arrangement to probe the drag force of the fluid, by understanding the trap strength (calibrating using a low frequency signal) one can measure the drag force experienced by the local fluid [44]. I

For any discussion of fluid flow its important that we know the fluid regime which is given by the Reynolds number. For a sphere submersed in a moving fluid of velocity  $U$  this is given by:

$$Re = \frac{\rho U D}{\mu} \quad (6.8)$$

Where  $D$  is the sphere's diameter, and  $\rho$  and  $\mu$  are the fluid's density and viscosity respectively. In our case we do not have a fluid moving around a sphere but a sphere moving through the fluid at some velocity  $U$ , assuming a no-slip boundary condition we can model the fluid velocity profile based on the velocity of the particle. Assuming that for now the fluid properties are unaffected by the rotating particle we see that for an individual sphere the Reynolds number can only change due to increasing/decreasing the fluid velocity. The fluid velocity is directly proportional to the particles rotation rate for low Reynolds numbers [45]. Given the small size of the particles used ( $1 - 10\mu m$  in diameter), and the relatively low rotation rates that are possible with an optical tweezer, for the case of our analysis the Reynolds number will not never be large enough to consider factors such as turbulence. There are two possible avenues for generating shear flow with a trapped particle; rotation of birefringent particles, and fluid flow

induced by particle motion.

Rotating birefringent particles are the more common method for generating and measuring fluid flow in a solution. To see if we can even achieve the theoretical maximum shear rate, Vaterite spheres were synthesised (see Sec.6.6) submerged in water and trapped with the 1064 nm laser at set to 450 mW. The rotation frequency was determined using the QPD, and the particle sizes were computed by image analysis. With the particle size and rotation frequency, the tangential rotation speed is calculated via:

$$u(r) = \frac{\pi}{4} \frac{d^3}{r^2} \omega \quad (6.9)$$

Where  $d$  is the particle diameter,  $\omega$  is the rotation frequency reported by the QPD, and  $r$  is the distance from the particle's centre. Using Eq.6.9 we calculated the fluid flow radiating outward from the centre of the sphere. The shear rate can then be computed as the partial derivative fluid flow (assuming shearing is generated purely by the flow field). This approach was used previously with liquid crystal rotors [4]:

$$\dot{\gamma}(r) = \left| \frac{\delta u(r)}{\delta r} \right| = \frac{\pi}{2} \frac{d^3}{r^3} \omega \quad (6.10)$$

One would expect that we set some reference distance where the fluid flow would be considered zero. However, at a microscopic level we are more concerned by the fluid shear for an individual nucleation event. We are essentially computing what the shear rate would be for a small volume of fluid between two moving parallel plates. This is similar logic to Mura and Zaccione's work where they considered the shear on a subcritical nucleus in a flow field [2]. They go further in depth to discuss the impact of material transport, overall coming to the conclusion that increasing shear rate leads to an increase the nucleation rate up till some maximum.

### 6.7.1 Estimation of fluid flow around a rotating particle in bulk fluid

First we determined the upper rotation rate that could be achieved using both Vaterite and liquid crystal spheres. Vaterite samples were synthesised according to [5], [46] (see sec. 6.6), and then suspended in distilled water. A sample of 200  $\mu L$  was pipetted and

a single microsphere was captured via a circular polarised beam.

Due to Van der Waal's forces some of the microspheres were stuck together, fortunately individual sphere's were still present. Individual microspheres were trapped and their rotation rate was determined by looking at the peak frequency component of the collected power spectrum. Due to their anisotropic scattering the QPD signal will oscillate periodically. After taking the Fourier transform of the QPD signal the power spectrum has distinctive peaks at integer multiples of the rotational frequency. The largest peak is often twice the rotational frequency which is due to the polarization modulation of the scattered field, the first peak is due purely to the rotation of vaterite sphere [39]. An example of this behaviour is shown in fig. 6.8.

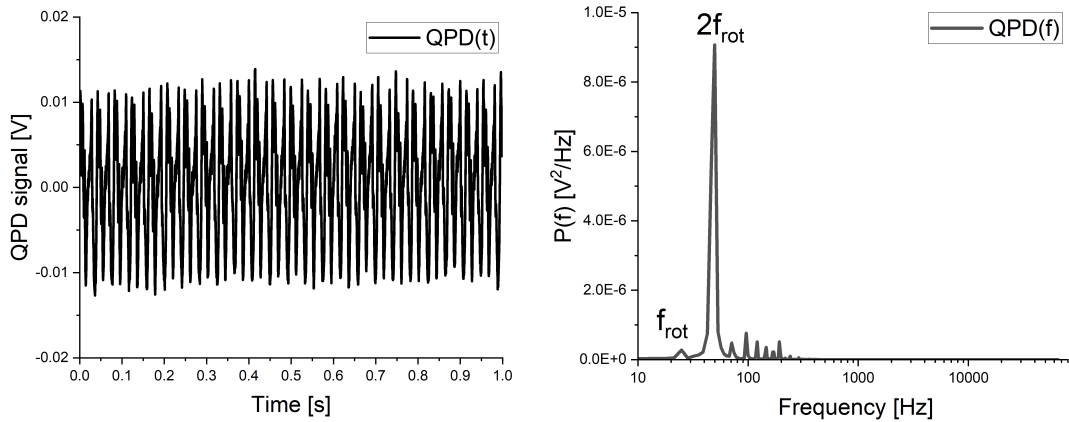


Figure 6.8: Example of QPD signal being converted from the time domain to the frequency domain. (left) Raw signal collected from the QPD over the 1st second of its trajectory showing a periodic spacing with a period of  $1/f_{\text{rot}}$ . (right) Power spectrum of the QPD signal, the y-axis is a linear scale to demonstrate the clear peaks in the power spectra. The rotational frequency is the first instance of a peak forming, and after that the peaks appear in integer multiples of  $f_{\text{rot}}$

The accuracy of the rotational frequency is dependent on the sample rate of the QPD and the sample duration [47]. With higher sampling rates resulting in a wider frequency window (see Sec.???) and longer sampling durations resulting in more distinct rotational peaks. The default QPD sampling rate is  $2^{17} \text{ Hz}$  which is more than adequate for detecting even the slightest low frequency signals. And the default sampling duration was  $3 \text{ s}$  which for most cases gave us clear distinct peaks for even relatively low rotational frequencies. After trapping a vaterite microsphere the power spectrum was recorded and

the rotation frequency was acquired. This was repeated several times for each sphere trapped, to confirm that the rotational frequency was constant and that the sphere had reached its maximum rotation rate.

After computing the rotational frequency the radial fluid speed could be estimated using Eq. (6.9). From there we can estimate the shear flow experienced by a small volume of fluid within the flow field (see Eq.(6.10)). Here we only consider the fluid flow as it propagates outward from the axis of rotation. While the cover slip will have some effect fluid flow it is difficult to quantify the effects of a hard boundary on a rotating object when the boundary is perpendicular to the axis of rotation.

From Fig.6.9 there is not a strong relationship between particle size and rotation rate, this is contrary to much of the theoretical predictions that predict an exponential decay with particle size. This can be in part due to the fact that synthesising perfectly spherical spheres that have uniform birefringence across the whole population is difficult. Despite our best efforts at controlling the growth rate the smallest particle ever synthesised was around  $3 \mu m$  in diameter. The Vaterite spheres would often stick together while suspended in water after a short period of time. The fastest reported rotation rate within a fluid was by [3] that achieved a rotation rate of  $5 kHz$ , this is plotted in Fig 6.9. In addition we added the results from [5] as a more realistic example.

The optimal shear rate predicted by [1] is plotted on Fig. 6.9(b), the outer dotted lines represent the point when the nucleation rate is less than 90% of the maximum. We can visualise the fluid around the rotating sphere by dividing it up into radial sections. Assuming the sphere is rotating sufficiently quickly there are three sections of concern, as demonstrated by fig. 6.10. The fluid close to the sphere experiences a shear rate that is far greater than the optimal shear rate, in which case nucleation is suppressed [2]. Secondly, there is a region of fluid that experiences a shear rate close to the optimal value ( $\pm 5\%$ ) where the nucleation rate is enhanced significantly compared to the bulk fluid. Lastly, beyond the optimal region the shear rate drops off exponentially in which case the nucleation rate is barely different compared to the bulk fluid.

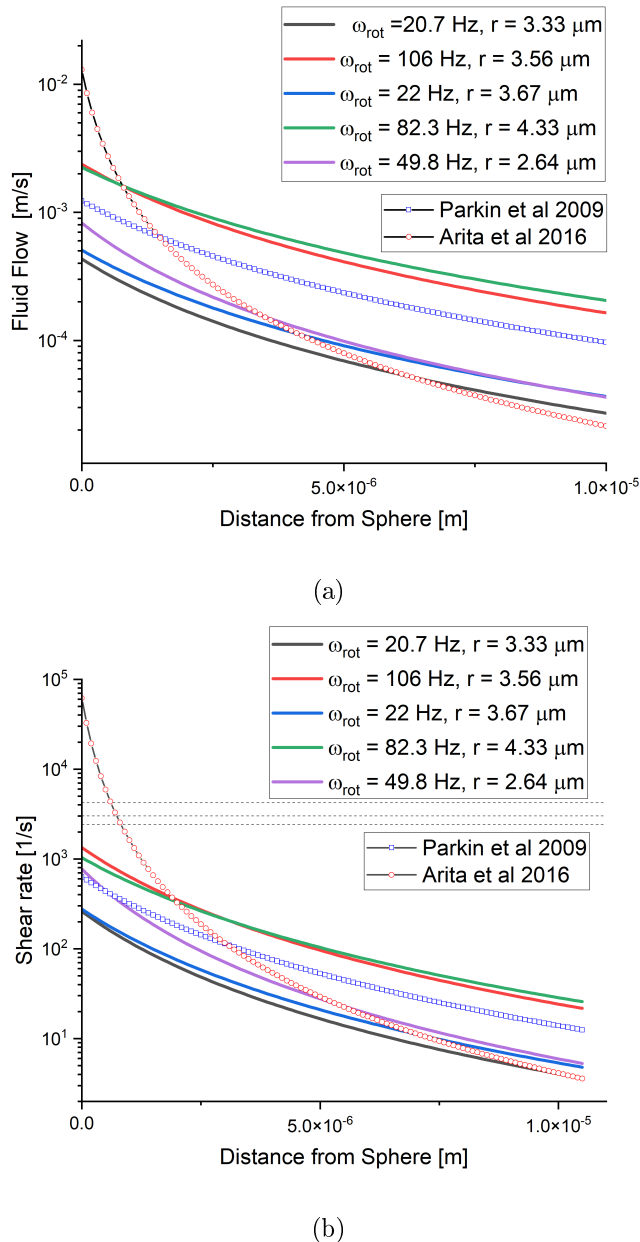


Figure 6.9: (Top) Fluid flow radiating out from the surface of a rotating Vaterite sphere. (Bottom) Shear rates computed using Eq. 6.10, optimal shear rate is of  $3000 \text{ s}^{-1}$  is indicated by the dotted line. Vaterite radii and rotation frequencies are shown, the laser power was kept constant at 450 mW. Reported rotation rates, and their corresponding fluid flow and shear rates, for Vaterite are also plotted alongside lab results. Results from [3], [5] are included as well.

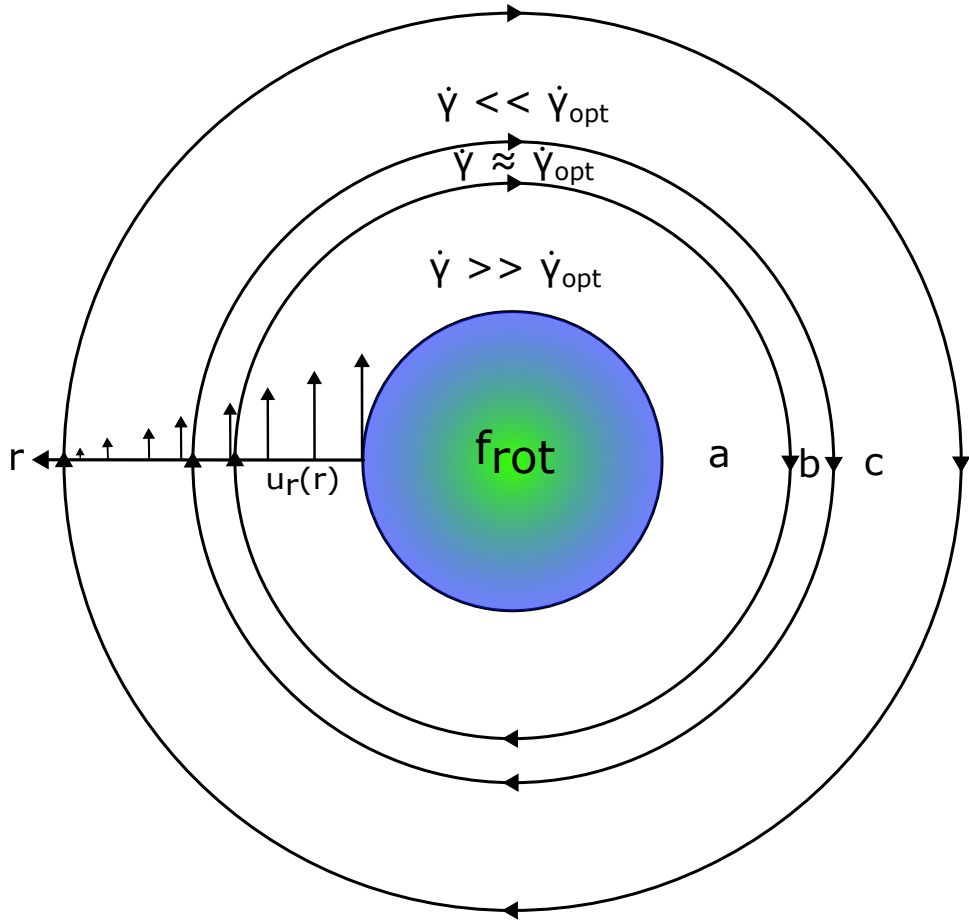


Figure 6.10: Diagram demonstrating how fluid shear rate varies radially from a rotating sphere (rotation rate =  $f_{rot}$ ). (a) the shear rate exceeds the optimal shear rate ( $\dot{\gamma}_{opt}$ ) and suppresses the nucleation rate. (b) shear rate is close to the optimal amount, enhancing the nucleation rate. (c) shear rate is far below the optimal amount and the nucleation rate is comparable to the bulk fluid.

## 6.8 Rotating spheres in Supersaturated solution

If rotation rates in bulk solution are insufficient then a rotating sphere close to an artificial barrier may be able to improve the shear rate of the surrounding fluid. Of course placing a solid barrier in a supersaturated fluid may well encourage nucleation somewhere on the surface outside of our control. Instead we chose to use the droplet edge of the supersaturated solution, while not a hard barrier per say, the molecular mobility close to the droplet edge is reduced due to surface tension. Furthermore, it has been shown through multiple results that nucleation is enhanced at the air-solution

interface [23], [48], [49].

Estimating the distance from the trap focus to the cover slip is difficult to measure directly, often requiring one fits a complex Lorentzian curve to the recorded power spectra in order to measure the fluid drag from being in close proximity to the cover slip [47]. We estimate that the vaterite must be at least  $15 - 20 \mu m$  from the cover slip for us to reliably trap them. The contact angle between the cover slip and solution was previously measured in [50], while being loosely dependent on the supersaturation the measured contact angle for supersaturated solutions was between  $30^\circ$  and  $35^\circ$ . This is shown in fig.6.11.

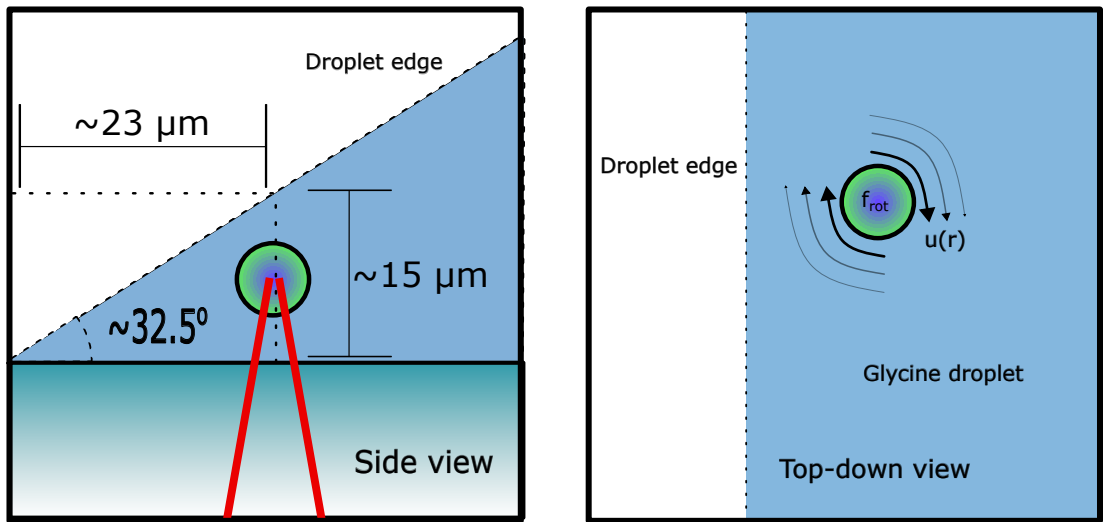


Figure 6.11: Diagram of optical trapping set up for rotating birefringent particles in a supersaturated solution. Left: side view of the trapping set up showing the location of the trap focus at the edge of the droplet of a supersaturated solution. The approximate contact angle (calculated by [50]) is used to provide a scale of how close a trapped particle could be located. Right: top down view of the glycine droplet with a trapped birefringent particle shown close to edge of the trap. As the particle rotates the drag force from the surrounding fluid generates a flow field around itself (see Eq. 6.9).

Supersaturated solutions of glycine and water were prepared and stored in an incubator at  $40^\circ C$  prior to use. When ready to be studied  $15 \mu L$  of vaterite suspension was pipetted into the solution and  $20 \mu L$  of the combined solution was pipetted onto the cover slip. A Vaterite sphere was located, trapped, and moved to the droplet edge where the solution meets the cover slip. This removed the need for hydrophilic coatings

to achieve a flat fluid layer (as used by [23], [51]).

Particle sizing was achieved by converting the particle diameter from pixels to physical units within an accuracy of  $\pm 0.05\mu m$ . The QPD was used to measure the frequency of fluctuations in the QPD signal. After measuring the rotational frequency the sphere was left to rotate for a period of ten minutes after which, if no nucleation event was observed the particle was released. The overall results are catalogued in table 6.1.

Table 6.1: Results from rotating Vaterite within supersaturated solution of  $H_2O$  and Glycine. Solubility concentration for Glycine at  $16^\circ$  was  $C^* = 0.2016g/g$

Super Saturation	Particle radius [ $\mu m$ ]	$\omega$ [Hz]	Nucleation [ $\checkmark/\times$ ]
1.01	2.34	10.4	$\times$
	3.26	8.46	$\times$
	5.67	9.63	$\times$
1.14	1.89	1.23	$\times$
	3.75	3.54	$\times$
	4.35	4.86	$\times$
1.4	1.59	0.00	$\times$
	3.47	0.00	$\times$
	6.24	0.00	$\times$
1.45	3.68	0.00	$\times$
	5.43	0.00	$\times$
	6.32	0.00	$\times$
1.49	1.52	0.00	$\times$
	4.76	0.00	$\times$
	7.27	0.00	$\times$

It should be noted that rotational frequencies equal to  $0.00\text{ Hz}$  are not due to a rounding error. Simply looking at the live video shows no rotation of the vaterite particles, and even looking at the QPD signals shows no discernable fluctuations that would arise due to rotation. Trying to trap a particle close to the edge proved more challenging than expected. Unlike in previous reports where the beam is focused at the upper edge of the droplet [23], [48], [52], we attempted trapping in close to the contact point of the droplet and the cover slip.

It is suspected that trapping is much harder at the interface due to increased surface tension and unpredictable scattering forces. The closest we could trap a microsphere to the droplet edge was in the range of  $5 - 10\mu m$ , at that distance the fluid flow is so low

## Chapter 6. Shear Induced Nucleation

that even the presence of a hard boundary would be insufficient for shearing the fluid. Furthermore, as is evident in Table 6.1, the rotation rate drops off significantly with increased supersaturation, due to higher fluid viscosities. While in theory a sufficiently focused laser could rotate any microsphere to a fast enough to reach the shear rate predicted by [1] the localised intensity would be so large that even using  $D_2O$  would see a significant increase in temperature.

It is not impossible that fluid shearing could be used in the future to localise nucleation; but from these results, using individual micro-rotors is not an appropriate method due to two key factors. Firstly, the area of influence is far too small to see any noticeable increase in the nucleation rate this is demonstrated most clearly in fig. 6.9. Due to the exponential decay in the expected shear rate it is very difficult trying to shear a large volume of fluid. Even if the optimal shear rate at a micro-level was an order of magnitude less than what was predicted by [1], only a small volume of fluid would even experience that shear rate. In order to properly understand the microscopic effects of fluid shear a method of localised shearing over a larger fluid volume is necessary.

Secondly, increased fluid viscosity significantly reduces the limits the maximum rotation rate possible. As indicated by 6.1, the rotation rate achievable by a vaterite sphere falls off significantly with increasing supersaturation. Experimental estimations of relative viscosities showed a 12% increase when looking at undersaturated glycine solutions ( $S \approx 0.34$ ) [53]. As far as we are aware there are no reported fluid viscosities for higher supersaturations. Extrapolating the results from [53] suggests that a saturated solution would have a 35% increase in fluid viscosity (compared to pure water). This also does not account for any other factors such as the fact that close to a boundary a rotating particle will experience a reaction torque from the stationary surface [45].

If multiple micro-rotors could be trapped in close proximity to one another they could create a large region of fluid where nucleation is more likely than the bulk fluid. Because optical torque is not contingent on the fluid properties the only limiting factor would be the total angular momentum transferred to each particle. Micro-rotors have been created that allow for precise control of suspended micro-particles [54] and could potentially be used to generate sufficient shearing. However these could not be used in

this project as we lacked the necessary hardware to form multiple gradient traps.

## 6.9 Nucleation with a Stationary and Moving Beam

As mentioned previously, shearing via optical rotation did not result in any localised nucleation events even while in the proximity of the droplet edge. An alternative approach was suggested, using a galvano mirror to move a particle quickly through a supersaturated solution. Preliminary calculations suggested a particle moving rapidly through a fluid could produce significantly greater shear rates (see *Appendix X.X* for breakdown) than a rotating particle. While a particle is within the optical trap the gradient forces are significantly reduced meaning simply trapping a particle is insufficient for inducing nucleation [50]. This is why we did not see any nucleation events while rotating the vaterite, there is not a large gradient force to draw in material.

During initial testing using silica beads we found that even in undersaturated solutions the optical trap would produce a crystal nucleus when the trap was empty. This has been reported prior [23], [51], but what is more interesting is how the beam's motion influenced the growth of the nucleus.

### 6.9.0.1 Choice of Crystal growth rate units

The growth rate of a crystal can be described using different units depending on the situation. For example, seed crystals often use growth units in the form of *length per unit time*. This can either be used to describe the overall length of the longest edge of a crystal, or to describe how individual faces grow separately. This works well for crystals with a clear morphology, in regards to laser induced nucleation the crystal growth is heavily influenced by the local fluid conditions meaning tracking the length of an individual face is challenging. Instead we utilise image analysis software such as imageJ to measure the area of the crystal after each frame to get a rough estimate of the crystal growth rate in units of *length<sup>2</sup> per unit time*. With the addition of the contact angle information from [50] we can approximate the crystal height based on how close it is to the droplet edge.

### 6.9.1 Stationary beam

It's well known that a supersaturated solution can nucleate if irradiated by a focused beam with sufficient power [51]. First we look at how a laser induced nucleation event unfolds using a stationary focused beam. The laser was focused at the edge of a  $20\mu L$  droplet consisting of water and dissolved glycine ( $S = 1.03$ ). The solution was monitored for 10 minutes, if a nucleation event was observed the event was recorded using a high speed CCD. If no nucleation event was observed after 10 minutes the solution was disposed of and a new sample was prepared. After ten repeats only 30% of the samples observed a nucleation event at the focus. All of which displayed similar growth behaviour to one another.

Consider Fig. 6.12, the frames taken from a nucleation event, the beam is a stationary being  $\approx 3.5\mu m$  from the droplet edge. After a period of roughly 5 minutes a nucleus forms at the trap focus, growing quickly (growth rate was approximated using imageJ to be on the order of  $700 \mu m^2/min$ ) from the focal point of the trap until after roughly 6 seconds the crystal escapes. A likely reason that the trap is escaped is due to the fact that crystal is far too large to be held in place and is in fact still growing as the solution is supersaturated. Based on the contact angle measurements from [50], the droplet height could not have been any more than  $2 - 5\mu m$  at the trap focus.

Comparing to previous literature using optical tweezers shows that the growth rate is only loosely connected to the solutions supersaturation. Crystal growth rates for a solution of glycine and water ( $S \approx 1.00$ ) was found to vary from as much as  $3900\mu m^2/min$  to as low as  $675\mu m^2/min$  [50]. The reason for such high crystal growth rates is due primarily to the tweezer focus bringing in material due to gradient forces. A study of glycine crystals in water found that for a similarly supersaturated solution the growth rate along the 011 face was around  $0.1 \mu m/min$  where as the 010 face was found to have a growth rate of around  $0.01 \mu m/min$ . While its difficult to extrapolate an exact area growth rate from these results we can approximate that if the we looked directly perpendicular to the crystal growth the area would increase at  $\approx 0.02 \mu^2/min$  (see X.X for a breakdown of this approximation).

The key take away to remember is that the beam has no influence over the crystal

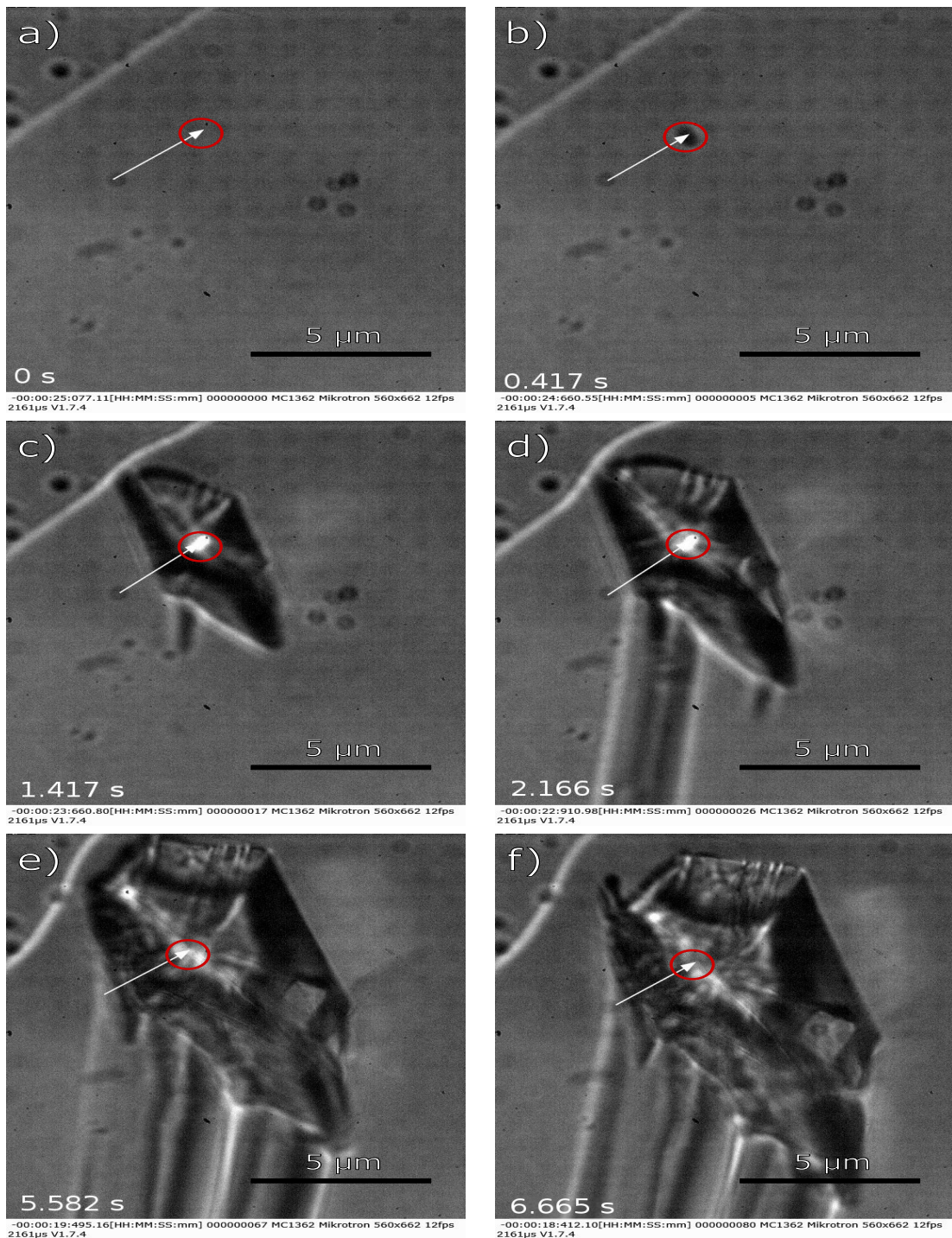


Figure 6.12: Laser induced nucleation at the edge of a droplet of supersaturated glycine solution. (b) shows the first instance of a crystal nucleus, growing quickly through (c)-(e) until after 6.665 s the crystal begins to escape the trap.

shape, instead it grows outward from the trap focus. Furthermore, due to the fact that the solution is supersaturated the crystal growth cannot be contained to the trap focus. Instead the crystal escapes as its size exceeds the trap focus.

### 6.9.2 Moving Beam

To test if a rapidly moving silica bead could generate the necessary shear rate for crystal nucleation we wanted to see if a trapped silica bead could be trapped and moved in an aqueous solution.  $20 \mu L$  of glycine and water ( $S = 1.03$ ) was added to  $10 \mu L$  of a dilute water-silica mixture making the solution unsaturated ( $S \approx 0.7$ ). However, due to the beam's motion we instead encountered unexpected growth behaviour.

Shown below in Fig. 6.13 where we have the laser focus moving in a small elliptical pattern. While nothing is seen directly entering the focus a nucleus forms close to the droplet edge, unlike in fig. 6.12 the crystal does not grow out from the focal point evenly. Due to the galvano mirror, the crystal is simultaneously being moved by and growing around the focal point of the trap. Because of this the crystal nucleus lacks a clear morphology at first. Until roughly  $20 s$  the crystal reaches a almost prismatic structure, with further irradiation increasing the size.

Interestingly the galvano-mirror allows the trap to impart a slight torque on the crystal, as shown in fig. 6.13(c) and (d), where even though the crystal is not directly in the trap focus it rotates in the  $x - y$  plane and gets trapped again at a corner. The rotation could not be due to fluid flow close to the surface of the crystal as the dipole moment of individual water molecules is too small to be influenced by an optical trap. In figs.6.13(e) and (f), the crystal growth becomes localised to the corner. The area growth rate between figures 6.13 (a) and (d) was approximated using imageJ at  $45.03 \mu m^2/min$ , where as between figures 6.13(e) and (f) the growth rate at that particular edge was estimated at  $42.10 \mu m^2/min$ .

Nucleation in undersaturated conditions has been reported previously in  $D_2O$  [51] and  $H_2O$  [50], though not involving a moving beam. This modification allows for the crystal growth to be localised to a specific region of the bulk crystal whereas with a stationary beam there is no control over the crystal morphology. In fact this allows for

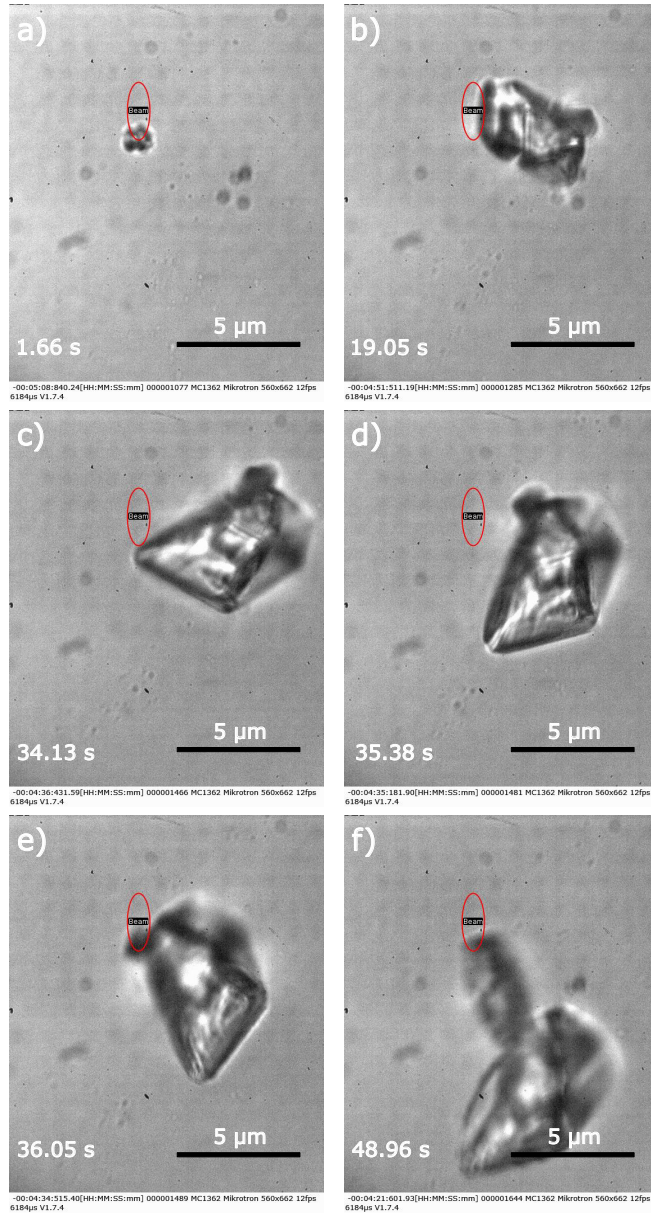


Figure 6.13: Frames from a longer video depicting the growth of a nucleus using a moving beam. Beam power is kept at 700 mW and the supersaturation was estimated at  $S=0.86$ . Initially the crystal shape is amorphous (a) but eventually reaches a more regular shape (b). This crystal is still influenced by the optical trap as even when not directly irradiated by the laser the crystal rotates between (c) and (d). When the laser is focused on a corner the crystal growth is localised to that region, resulting in an elongated section forming between frames (e) and (f).

a much finer control over the exact shape of the crystal nucleus, in some cases allowing for growth out of the viewing plane as shown in fig. 6.14.

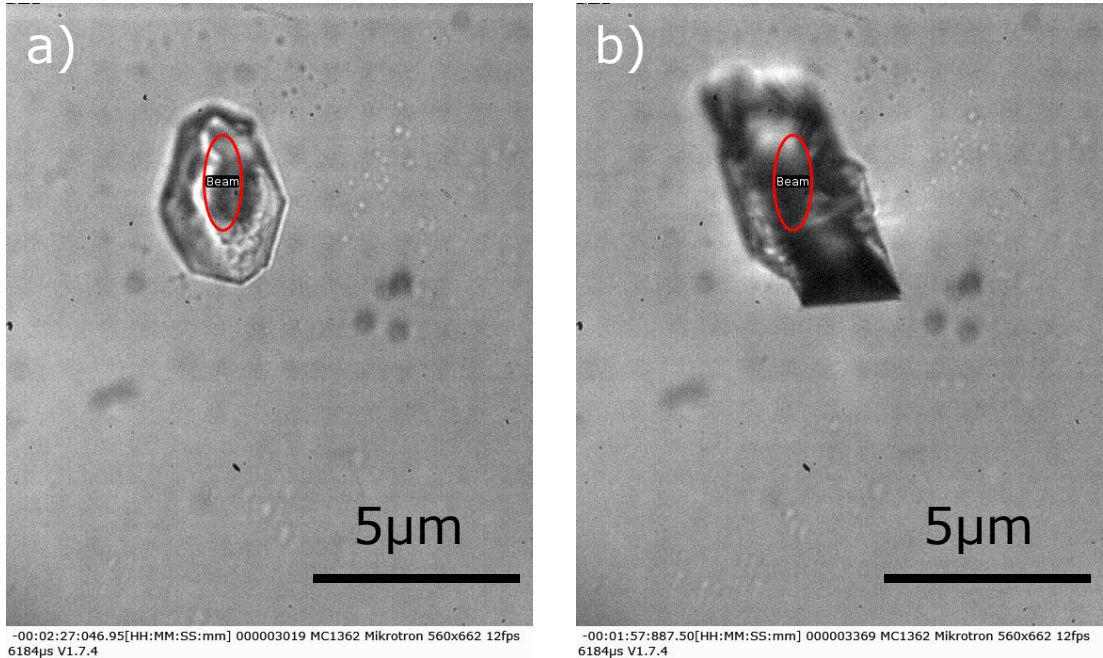


Figure 6.14: Interesting crystal growth on the surface of an existing crystal. Initially the crystal surface seems flat (a) but eventually a different crystal structure grows out off the surface (b).

Where a large outgrowth forms on the surface of a nucleus, over a period of 30 s the outgrowth develops into a rhombic crystal structure. The unique crystal growth demonstrated is likely a factor of the moving beam focus, but this raises a question over how the laser can localise the growth only around the focus and why the crystal does not grow or shrink when not directly within the trap. There should be some material that is being drawn into the trap as it scans across the camera frame.

### 6.9.3 Direct trapping of Glycine clusters

In a repeat experiment a solution similar to sec. 6.9.1 was made up, but without any silica micro-spheres. Once again the beam was focused close to the droplet edge, this time the galvano mirror was scanning a circular path (as shown in fig. 6.15). After a few minutes of irradiation droplets were seen entering the camera frame. Because no silica

## Chapter 6. Shear Induced Nucleation

had been added, and that the solutions were filtered, these droplets had to be from the glycine solution. Trapping individual droplets did not result in immediate nucleation even after several minutes being trapped. Trying to bring two droplets together resulted in nucleation between the two droplets, compared to 6.9.1 & 6.9.2 the growth is much slower, taking nearly 40 seconds before the crystal structure becomes clearer.

The fact that these droplets can be trapped indicates they must have a higher refractive index than the surrounding solution. Previous reports have shown that a focused trap will draw in solute material from the bulk [55], [56]. This suggests that the droplets observed are concentrated spheres of glycine, which also explains how nucleation was initiated when those two spheres were brought into contact with one another. The droplets must be providing material for the crystal growth. It has been shown that the concentration of glycine solution is correlated with the refractive indices of the liquid [56], [57]. This suggests that we could measure the concentration of individual droplets based on the trapping strength of each droplet.

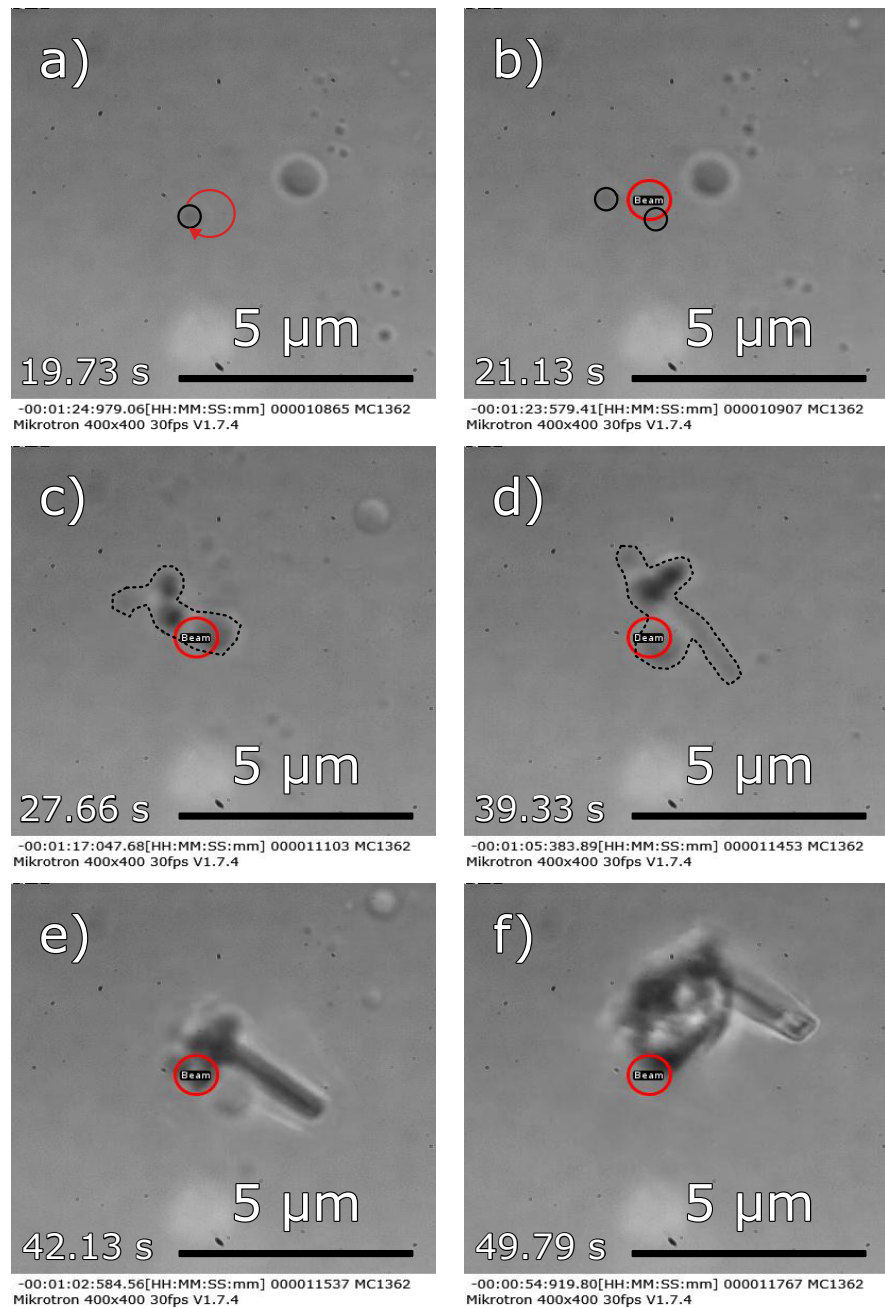


Figure 6.15: Frames from a longer video demonstrating the trapping of a glycine droplet. Solution is undersaturated glycine and water ( $S = 0.86$ ), with the laser power set at 750 mW. (a) shows a trapped droplet (outlined in black) being brought into contact with a larger droplet. (b) upon contact a nucleus can be seen between the two droplets. The growth is rather slow with the crystal having no clear defined morphology through (c) and (d). Between frames (e) and (f) the larger droplet finally joins the main crystal.

#### 6.9.4 Influence of a moving beam front on seed crystals

One potential application of this phenomena would be in using a moving the moving beam front as a method for shaping the final crystal morphology. Therefore, we wanted to test if a moving beam front could have any influence on the shape of a seed crystal submerged in a bulk solution. Glycine seed crystals were grown via evaporative crystallisation over night. The resultant crystals were as wide as  $0.5\text{mm}$  in some cases. Individual crystals were collected and suspended in a water + glycine solution ( $S = 1.001$ ) and the laser was scanned along a narrow linear path. It should be noted that the seed crystal was fully submerged in the solution, meaning that there is no interface between the air and solution close to the seed. Five separate repeats were conducted, all demonstrating similar behaviour to one another.

As shown by fig. 6.16 the laser does not in fact promote crystal growth but instead forces the crystal to dissolve into the bulk solution. The dissolution rate is not as substantial as the growth rate seen in previous sections. It takes over 20 minutes for the for the crystal surface to dissolve more than a few microns. Furthermore we do not report any sightings of droplets close to the surface of the crystal nor do we see anything enter the optical trap.

This has some implications: Firstly, the lack of supposed glycine droplets suggests that the presence of an interface is crucial in order to promote the formation of these droplets. This is consistent with previous reports on laser nucleation, where a air-solution or solution-glass interface is necessary for the trap focus to have any noticeable effect on the solute [23], [51], [56]. Secondly, the fact that the seed crystal dissolved in a saturated solution suggests that this could be due to a localised heating effect. A commonly used heating model for optical tweezers is the Peterman model [58] which accounts for the lateral distance between the optical trap and a local heat sink (such as the glass cover slip or microscope objective). Even with the heat sink the predicted temperature rise in pure water would be around  $5 - 10K$ . The fact that the seed crystal dissolves so slowly could simply be due to the fact that the local heating is lessened by the moving beam front.

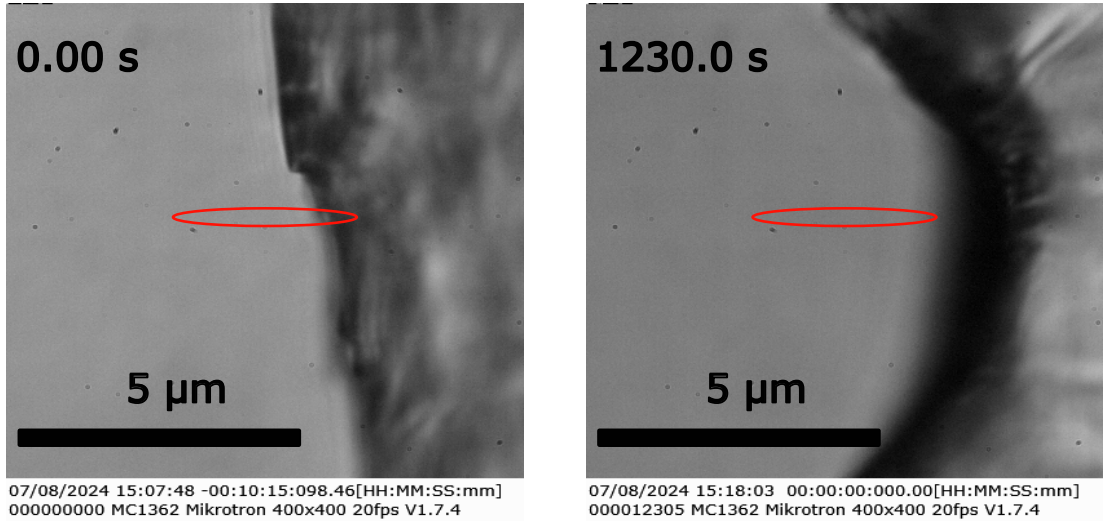


Figure 6.16: Frames from a seed crystal being irradiated by a scanning laser. The laser path is shown below in red. Initially the crystal edge is nearly perpendicular to the laser path. Over the course of nearly twenty minutes the crystal around the laser has dissolved leaving a concave indent.

## 6.10 Summary of Moving Beam Phenomena

To summarise, the introduction of a moving beam helps to accelerate the local growth of a newly formed crystal. It seems that this phenomena will only occur when close to interface between the solution and air. We note the presence of droplets that can sometimes be seen entering the trap, though this is not always necessary for a nucleation event to occur. A plausible description of the phenomena is described thusly.

Initial nucleation is similar to typical optical trapping induced nucleation, with the air solution interface limiting the molecular mobility of the solute molecules [23], [49], [56]. The moving beam front can influence the motion of the nucleus initially, but eventually the drag force means the crystal is not moved by the optical trap. Localised crystal growth occurs when the trap is close to or partially over the interface of the crystal (see fig. 6.17(a)). This suggests that the laser itself is bringing in new solute material that can then adhere to the crystal surface. Interestingly even when the crystal growth is localised to a small section of the crystal we do not observe the crystal dissolving. This is consistent with other observed laser induced nucleation results, where as long as the laser is active the crystal remains stable within the solution [23], [49]–[51]. It

does raise further questions however, mainly in an undersaturated solution is a moving beam front able to increase the size of the formed nucleus compared to a stationary beam? Additionally, it raises the question about what the role the 'glycine droplets' play in the nucleation process.

As shown in 6.9.3, the optical trap can manipulate these droplets similar to microspheres. When in close proximity to the trap these droplets are brought towards the crystal surface (see fig. 6.17(b)). We have already suggested that these droplets must contain glycine as they are to large to be a silica microsphere, and the solutions were filtered prior to being studied. The droplets provide material that grows the crystal around that region (see fig. 6.17(c)). Eventually the local solution is either depleted of solute material or the crystal front has grown to fully encompass the trap, preventing further growth (see fig. 6.17(d)).

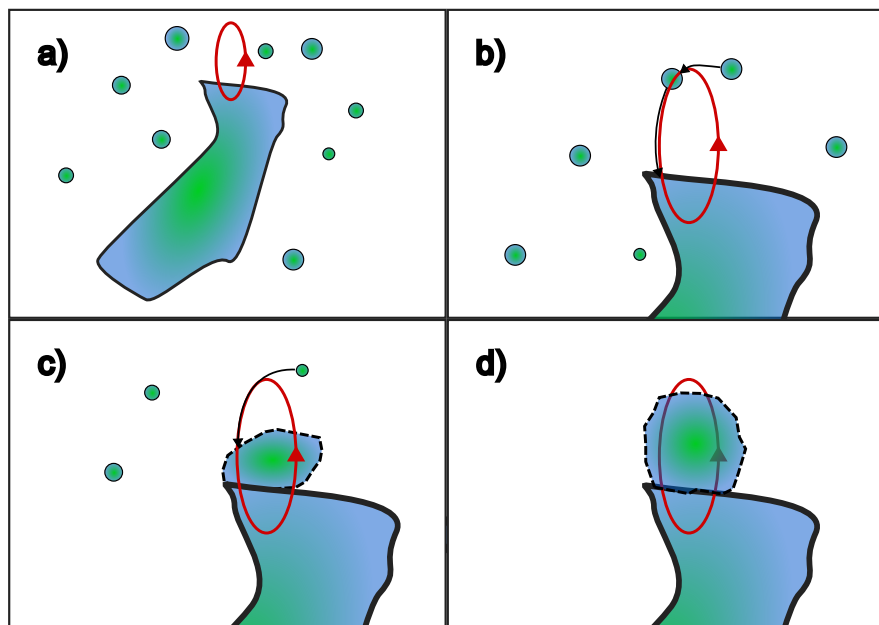


Figure 6.17: Diagram outlining how a moving beam assists in the growth of a crystal nucleus. (a) a crystal nucleus is partially trapped by a moving beam with solute droplets close to its surface. (b) droplets close to the laser focus can be drawn in by gradient forces and moved towards the crystal surface. (c) the laser brings in material that is then deposited on the surface of the crystal. (d) eventually the crystal area either fully surrounds the laser focus or the solution surrounding the laser is depleted of solute material.

## Chapter 6. Shear Induced Nucleation

What remains unclear is why the solution interface is necessary for localised crystal growth. We know that the glycine droplets will form when the laser is close to the glass-solution interface [48], [56], [59]. This is consistent with our results as being able to image the droplet edge requires that the laser is brought close to the cover slip. However it is not clear how exactly these droplets contribute to localised crystal growth as in sec. 6.9.2 no droplets are seen entering the trap. It seems likely that the presence of droplets is necessary as we see that the seed crystals dissolve while there are no droplets present.

There are still several factors that need to be investigated. Firstly, there is the question of what conditions result in the production of concentrated droplets, it is not clear if the presence of a laser is required or if these droplets naturally occurring. Prior literature would suggest that the laser is required [23], [55], but this would not explain why in many cases the droplets are found far outside the influence of the optical trap. It has been shown that phase separation occurs when a trap is focused close to the cover slip [48], [56], [59], but there has been no cases of nucleation occurring at the cover slip. Furthermore these experiments all occurred in supersaturated condition ( $S \geq 1.50$ ) with a much wider focus ( $NA \leq 1.00$ ) whereas our results occurred in undersaturated conditions with a tighter focus. We did not not any occurrence of a phase separation as reported by [48], [56], [59] and yet we see the appearance of droplets that we surmise are partially constructed of glycine.

Secondly, there is the question of how these droplets supply material to the bulk crystal. In some instances it is clear that the droplets are being drawn into the trap, however, in other instances while there are no droplets close to the vicinity of the optical trap the crystal continues to grow. If these droplets are a necessary precursor to induce crystal nucleation then understanding how they provide materials to the bulk crystal may help with our understanding of the kinetics of multi-step nucleation.

## 6.11 Conclusion

In conclusion, the experimental results from this chapter provide no affirmative evidence of shear induced crystal nucleation. This is in part due to the limited rotational speed that could be achieved using vaterite microspheres. Simply adding a micro-rotor to a supersaturated solution will not yield a significant fluid flow to induce crystal nucleation. Furthermore, the region in which the local shear rate is significant enough is so small that any nucleation events that could occur there may not grow large enough to be stable. This does not however, suggest that shear induced nucleation is impossible at a micro scale. In fact there have been several developments lately that allow for the precise rotation of multiple rotors to control the precise motion of silica beads [54]. This would allow for direct control of the shear rate within a given volume of fluid, allowing one to study the impact of fluid flow on a nucleus at a micro-scale.

On the other hand, the results utilising the galvano mirror have some interesting implications for future research into crystal nucleation using optical tweezers. We noted that a moving beam front is capable of localising the crystal growth around the beam focus in undersaturated conditions. Typically in laser induced nucleation the final crystal morphology is influenced primarily by the local fluid conditions [23], [50]. If this phenomena could be fully understood we could have a means of directly manipulating the morphology of any nucleating crystal. We noted that in undersaturated conditions the presence of droplets that could be trapped and later nucleated when brought into contact with one another. There remains some uncertainty over the role these droplets play in a nucleation event. Further research is also necessary to understand how the fluid and laser parameters (i.e. supersaturation and numerical aperture) impact the formation of these droplets. The fact that these droplets could be trapped suggests they have a higher refractive index to the solution, given that the solutions were filtered prior to irradiation dismisses that they could be dust particles. Prior literature suggests that optical trapping of a supersaturated solution can lead to the production of nano droplets [55], [56].

# Bibliography

- [1] R. Debuyschère, B. Rimez, A. Zaccione, *et al.*, “Experimental and theoretical investigation of nonclassical shear-induced nucleation mechanism for small molecule,” *Crystal Growth & Design*, vol. 23, no. 7, pp. 4979–4989, Jun. 2023, ISSN: 1528-7505. DOI: [10.1021/acs.cgd.3c00232](https://doi.org/10.1021/acs.cgd.3c00232).
- [2] F. Mura and A. Zaccione, “Effects of shear flow on phase nucleation and crystallization,” *Physical Review E*, vol. 93, no. 4, p. 042803, Apr. 2016, ISSN: 2470-0053. DOI: [10.1103/physreve.93.042803](https://doi.org/10.1103/physreve.93.042803).
- [3] Y. Arita, J. M. Richards, M. Mazilu, *et al.*, “Rotational dynamics and heating of trapped nanovaterite particles,” *ACS Nano*, vol. 10, no. 12, pp. 11 505–11 510, Dec. 2016, ISSN: 1936-086X. DOI: [10.1021/acsnano.6b07290](https://doi.org/10.1021/acsnano.6b07290).
- [4] K. Saito and Y. Kimura, “Optically driven liquid crystal droplet rotator,” *Scientific Reports*, vol. 12, no. 1, Oct. 2022, ISSN: 2045-2322. DOI: [10.1038/s41598-022-21146-y](https://doi.org/10.1038/s41598-022-21146-y).
- [5] S. J. Parkin, R. Vogel, M. Persson, *et al.*, “Highly birefringent vaterite microspheres: Production, characterization and applications for optical micromanipulation,” *Optics Express*, vol. 17, no. 24, p. 21944, Nov. 2009, ISSN: 1094-4087. DOI: [10.1364/oe.17.021944](https://doi.org/10.1364/oe.17.021944).
- [6] J. W. Mullin, *Crystallization*. 4th ed. Oxford: Elsevier Science Technology, 2001, 1611 pp., Description based on publisher supplied metadata and other sources., ISBN: 9780080530116.

## Bibliography

- [7] G. D. Botsaris, “Secondary nucleation — a review,” in *Industrial Crystallization*. Springer US, 1976, pp. 3–22, ISBN: 9781461572589. DOI: [10.1007/978-1-4615-7258-9\\_1](https://doi.org/10.1007/978-1-4615-7258-9_1).
- [8] J. Anwar, S. Khan, and L. Lindfors, “Secondary crystal nucleation: Nuclei breeding factory uncovered,” *Angewandte Chemie International Edition*, vol. 54, no. 49, pp. 14 681–14 684, Mar. 2015, ISSN: 1521-3773. DOI: [10.1002/anie.201501216](https://doi.org/10.1002/anie.201501216).
- [9] S. G. Agrawal and A. H. J. Paterson, “Secondary nucleation: Mechanisms and models,” *Chemical Engineering Communications*, vol. 202, no. 5, pp. 698–706, Jan. 2015, ISSN: 1563-5201. DOI: [10.1080/00986445.2014.969369](https://doi.org/10.1080/00986445.2014.969369).
- [10] J. Frenkel, “A general theory of heterophase fluctuations and pretransition phenomena,” *The Journal of Chemical Physics*, vol. 7, no. 7, pp. 538–547, Jul. 1939, ISSN: 1089-7690. DOI: [10.1063/1.1750484](https://doi.org/10.1063/1.1750484).
- [11] M. Volmer and Weber, “Keimbildung in ubersättigten gebilden,” *Zeitschrift für Physikalische Chemie*, vol. 119U, no. 1, pp. 277–301, Jan. 1926, ISSN: 0942-9352. DOI: [10.1515/zpch-1926-11927](https://doi.org/10.1515/zpch-1926-11927).
- [12] S. Karthika, T. K. Radhakrishnan, and P. Kalaichelvi, “A review of classical and nonclassical nucleation theories,” *Crystal Growth & Design*, vol. 16, no. 11, pp. 6663–6681, Oct. 2016, ISSN: 1528-7505. DOI: [10.1021/acs.cgd.6b00794](https://doi.org/10.1021/acs.cgd.6b00794).
- [13] M. Gharibeh, Y. Kim, U. Dieregsweiler, *et al.*, “Homogeneous nucleation of n-propanol, n-butanol, and n-pentanol in a supersonic nozzle,” *The Journal of Chemical Physics*, vol. 122, no. 9, Mar. 2005, ISSN: 1089-7690. DOI: [10.1063/1.1858438](https://doi.org/10.1063/1.1858438).
- [14] P. G. Vekilov, “The two-step mechanism of nucleation of crystals in solution,” *Nanoscale*, vol. 2, no. 11, p. 2346, 2010, ISSN: 2040-3372. DOI: [10.1039/c0nr00628a](https://doi.org/10.1039/c0nr00628a).
- [15] W. T. Lee, E. K. H. Salje, and M. T. Dove, “Effect of surface relaxations on the equilibrium growth morphology of crystals: Platelet formation,” *Journal of Physics: Condensed Matter*, vol. 11, no. 38, pp. 7385–7410, Sep. 1999, ISSN: 1361-648X. DOI: [10.1088/0953-8984/11/38/316](https://doi.org/10.1088/0953-8984/11/38/316).

## Bibliography

- [16] S.-T. Yau and P. G. Vekilov, “Direct observation of nucleus structure and nucleation pathways in apoferritin crystallization,” *Journal of the American Chemical Society*, vol. 123, no. 6, pp. 1080–1089, Jan. 2001, ISSN: 1520-5126. DOI: [10.1021/ja003039c](https://doi.org/10.1021/ja003039c).
- [17] A. E.S., V. Driessche, M. Kellermeier, *et al.*, *New Perspectives on Mineral Nucleation and Growth*. Springer International Publishing, 2017, ISBN: 9783319456690. DOI: [10.1007/978-3-319-45669-0](https://doi.org/10.1007/978-3-319-45669-0).
- [18] H. Fu, X. Gao, X. Zhang, *et al.*, “Recent advances in nonclassical crystallization: Fundamentals, applications, and challenges,” *Crystal Growth & Design*, vol. 22, no. 2, pp. 1476–1499, Nov. 2021, ISSN: 1528-7505. DOI: [10.1021/acs.cgd.1c01084](https://doi.org/10.1021/acs.cgd.1c01084).
- [19] J. R. Savage and A. D. Dinsmore, “Experimental evidence for two-step nucleation in colloidal crystallization,” *Physical Review Letters*, vol. 102, no. 19, p. 198302, May 2009, ISSN: 1079-7114. DOI: [10.1103/physrevlett.102.198302](https://doi.org/10.1103/physrevlett.102.198302).
- [20] P. R. t. Wolde and D. Frenkel, “Enhancement of protein crystal nucleation by critical density fluctuations,” *Science*, vol. 277, no. 5334, pp. 1975–1978, Sep. 1997, ISSN: 1095-9203. DOI: [10.1126/science.277.5334.1975](https://doi.org/10.1126/science.277.5334.1975).
- [21] K. G. Soga, J. R. Melrose, and R. C. Ball, “Metastable states and the kinetics of colloid phase separation,” *The Journal of Chemical Physics*, vol. 110, no. 4, pp. 2280–2288, Jan. 1999, ISSN: 1089-7690. DOI: [10.1063/1.477881](https://doi.org/10.1063/1.477881).
- [22] W. Ostwald, “Studien über die bildung und umwandlung fester Körper: 1. abhandlung: Übersättigung und Überkaltung,” *Zeitschrift für Physikalische Chemie*, vol. 22U, no. 1, pp. 289–330, Feb. 1897, ISSN: 0942-9352. DOI: [10.1515/zpch-1897-2233](https://doi.org/10.1515/zpch-1897-2233).
- [23] Z. Liao and K. Wynne, “A metastable amorphous intermediate is responsible for laser-induced nucleation of glycine,” vol. 144, pp. 6727–6733, 2022, ISSN: 0002-7863. DOI: [10.1021/jacs.1c11154](https://doi.org/10.1021/jacs.1c11154).

## Bibliography

- [24] K. Cao, J. Biskupek, C. T. Stoppiello, *et al.*, “Atomic mechanism of metal crystal nucleus formation in a single-walled carbon nanotube,” *Nature Chemistry*, vol. 12, no. 10, pp. 921–928, Aug. 2020, ISSN: 1755-4349. DOI: [10.1038/s41557-020-0538-9](https://doi.org/10.1038/s41557-020-0538-9).
- [25] H. Ye, Z. Zhang, and R. Wang, “Nucleation and growth of nanocrystals investigated by in situ transmission electron microscopy,” *Small*, vol. 19, no. 49, Aug. 2023, ISSN: 1613-6829. DOI: [10.1002/smll.202303872](https://doi.org/10.1002/smll.202303872).
- [26] P. Tan, N. Xu, and L. Xu, “Visualizing kinetic pathways of homogeneous nucleation in colloidal crystallization,” *Nature Physics*, vol. 10, no. 1, pp. 73–79, Dec. 2013, ISSN: 1745-2481. DOI: [10.1038/nphys2817](https://doi.org/10.1038/nphys2817).
- [27] J. Baumgartner, A. Dey, P. H. H. Bomans, *et al.*, “Nucleation and growth of magnetite from solution,” *Nature Materials*, vol. 12, no. 4, pp. 310–314, Feb. 2013, ISSN: 1476-4660. DOI: [10.1038/nmat3558](https://doi.org/10.1038/nmat3558).
- [28] M. A. Durán-Olivencia and J. F. Lutsko, “Mesoscopic nucleation theory for confined systems: A one-parameter model,” *Physical Review E*, vol. 91, no. 2, p. 022 402, Feb. 2015, ISSN: 1550-2376. DOI: [10.1103/physreve.91.022402](https://doi.org/10.1103/physreve.91.022402).
- [29] A. R. Finney and M. Salvalaglio, “Molecular simulation approaches to study crystal nucleation from solutions: Theoretical considerations and computational challenges,” *WIREs Computational Molecular Science*, vol. 14, no. 1, Nov. 2023, ISSN: 1759-0884. DOI: [10.1002/wcms.1697](https://doi.org/10.1002/wcms.1697).
- [30] D. B. Williams and C. B. Carter, *Transmission Electron Microscopy*. Springer US, 2009, ISBN: 9780387765013. DOI: [10.1007/978-0-387-76501-3](https://doi.org/10.1007/978-0-387-76501-3).
- [31] P. E. Champness, *Electron diffraction in the transmission electron microscope*, Aug. 2020. DOI: [10.1201/9781003076872](https://doi.org/10.1201/9781003076872).
- [32] N. D. Loh, S. Sen, M. Bosman, *et al.*, “Multistep nucleation of nanocrystals in aqueous solution,” *Nature Chemistry*, vol. 9, no. 1, pp. 77–82, Oct. 2016, ISSN: 1755-4349. DOI: [10.1038/nchem.2618](https://doi.org/10.1038/nchem.2618).

## Bibliography

- [33] E. T. Broadhurst, H. Xu, M. T. B. Clabbers, *et al.*, “Polymorph evolution during crystal growth studied by 3d electron diffraction,” *IUCrJ*, vol. 7, no. 1, pp. 5–9, Jan. 2020, ISSN: 2052-2525. DOI: [10.1107/s2052252519016105](https://doi.org/10.1107/s2052252519016105).
- [34] J. G. J. R. G.-S. A. M. I. P. Castillo, “Optical tweezers - fromn calibration to applications: A tutorial,” *Optics*, 2020. DOI: <https://doi.org/10.48550/arXiv.2004.05246>. [Online]. Available: <https://arxiv.org/abs/2004.05246>.
- [35] H.-I. Kim, I.-J. Joo, S.-H. Song, *et al.*, “Dependence of the optical trapping efficiency on the ratio of the beam radius-to-the aperture radius,” *Journal of the Korean Physical Society*, vol. 43, no. 3, p. 348, 2003.
- [36] S. N. S. Reihani, M. A. Charsooghi, H. R. Khalesifard, *et al.*, “Efficient in-depth trapping with an oil-immersion objective lens,” vol. 31, p. 766, 2006, ISSN: 0146-9592. DOI: [10.1364/ol.31.000766](https://doi.org/10.1364/ol.31.000766).
- [37] D. Konopacka-Łyskawa, “Synthesis methods and favorable conditions for spherical vaterite precipitation: A review,” *Crystals*, vol. 9, no. 4, p. 223, Apr. 2019, ISSN: 2073-4352. DOI: [10.3390/cryst9040223](https://doi.org/10.3390/cryst9040223).
- [38] Yugesha, S. Bhattacharya, and S. Ananthamurthy, “Characterizing the rotation of non symmetric objects in an optical tweezer,” *Optics Communications*, vol. 285, no. 10–11, pp. 2530–2535, May 2012, ISSN: 0030-4018. DOI: [10.1016/j.optcom.2012.01.055](https://doi.org/10.1016/j.optcom.2012.01.055).
- [39] F. Monteiro, S. Ghosh, E. C. van Assendelft, *et al.*, “Optical rotation of levitated spheres in high vacuum,” *Physical Review A*, vol. 97, no. 5, p. 051802, May 2018, ISSN: 2469-9934. DOI: [10.1103/physreva.97.051802](https://doi.org/10.1103/physreva.97.051802).
- [40] G. Volpe, O. M. Maragò, H. Rubinsztein-Dunlop, *et al.*, “Roadmap for optical tweezers,” *Journal of Physics: Photonics*, vol. 5, no. 2, p. 022501, Apr. 2023, ISSN: 2515-7647. DOI: [10.1088/2515-7647/acb57b](https://doi.org/10.1088/2515-7647/acb57b).
- [41] J. Millen, T. Deesawan, P. Barker, *et al.*, “Nanoscale temperature measurements using non-equilibrium brownian dynamics of a levitated nanosphere,” *Nature Nanotechnology*, vol. 9, no. 6, pp. 425–429, May 2014, ISSN: 1748-3395. DOI: [10.1038/nnano.2014.82](https://doi.org/10.1038/nnano.2014.82).

## Bibliography

- [42] P. Rodríguez-Sevilla, Y. Arita, X. Liu, *et al.*, “The temperature of an optically trapped, rotating microparticle,” *ACS Photonics*, vol. 5, no. 9, pp. 3772–3778, Aug. 2018, ISSN: 2330-4022. DOI: [10.1021/acspophotonics.8b00822](https://doi.org/10.1021/acspophotonics.8b00822).
- [43] G. Knöner, S. Parkin, N. R. Heckenberg, *et al.*, “Characterization of optically driven fluid stress fields with optical tweezers,” *Physical Review E*, vol. 72, no. 3, p. 031507, Sep. 2005, ISSN: 1550-2376. DOI: [10.1103/physreve.72.031507](https://doi.org/10.1103/physreve.72.031507).
- [44] R. M. Robertson-Anderson, “Optical tweezers microrheology: From the basics to advanced techniques and applications,” *ACS Macro Letters*, vol. 7, no. 8, pp. 968–975, Aug. 2018, ISSN: 2161-1653. DOI: [10.1021/acsmacrolett.8b00498](https://doi.org/10.1021/acsmacrolett.8b00498).
- [45] G. D. Bruce, P. Rodríguez-Sevilla, and K. Dholakia, “Initiating revolutions for optical manipulation: The origins and applications of rotational dynamics of trapped particles,” *Advances in Physics: X*, vol. 6, no. 1, Dec. 2020, ISSN: 2374-6149. DOI: [10.1080/23746149.2020.1838322](https://doi.org/10.1080/23746149.2020.1838322).
- [46] A. I. Bishop, T. A. Nieminen, N. R. Heckenberg, *et al.*, “Optical microrheology using rotating laser-trapped particles,” *Physical Review Letters*, vol. 92, no. 19, p. 198 104, May 2004, ISSN: 1079-7114. DOI: [10.1103/physrevlett.92.198104](https://doi.org/10.1103/physrevlett.92.198104).
- [47] K. Berg-Sørensen and H. Flyvbjerg, “Power spectrum analysis for optical tweezers,” vol. 75, pp. 594–612, 2004, ISSN: 0034-6748. DOI: [10.1063/1.1645654](https://doi.org/10.1063/1.1645654).
- [48] K.-i. Yuyama, T. Sugiyama, and H. Masuhara, “Millimeter-scale dense liquid droplet formation and crystallization in glycine solution induced by photon pressure,” *The Journal of Physical Chemistry Letters*, vol. 1, no. 9, pp. 1321–1325, Apr. 2010, ISSN: 1948-7185. DOI: [10.1021/jz100266t](https://doi.org/10.1021/jz100266t).
- [49] T. Sugiyama, T. Adachi, and H. Masuhara, “Crystal growth of glycine controlled by a focused cw near-infrared laser beam,” *Chemistry Letters*, vol. 38, no. 5, pp. 482–483, Apr. 2009, ISSN: 1348-0715. DOI: [10.1246/cl.2009.482](https://doi.org/10.1246/cl.2009.482).
- [50] J. Flannigan, “Optical tweezer and particle control of nucleation and growth at the microscale,” Ph.D. dissertation, University of Strathclyde, 2023. [Online]. Available: <https://pureportal.strath.ac.uk/en/studentTheses/optical-tweezer-and-particle-control-of-nucleation-and-growth-at->.

## Bibliography

- [51] T. Rungsimanon, K.-i. Yuyama, T. Sugiyama, *et al.*, “Crystallization in unsaturated glycine/d<sub>2</sub>o solution achieved by irradiating a focused continuous wave near infrared laser,” vol. 10, pp. 4686–4688, 2010, ISSN: 1528-7483. DOI: [10.1021/cg100830x](https://doi.org/10.1021/cg100830x).
- [52] T. Sugiyama and S.-F. Wang, “Manipulation of nucleation and polymorphism by laser irradiation,” *Journal of Photochemistry and Photobiology C: Photochemistry Reviews*, vol. 52, p. 100530, Sep. 2022, ISSN: 1389-5567. DOI: [10.1016/j.jphotochemrev.2022.100530](https://doi.org/10.1016/j.jphotochemrev.2022.100530).
- [53] P. Patyar, K. Kaur, and G. Singh, “Viscometric and spectroscopic studies on interactions of glycine with aqueous buffer solutions,” *Journal of Molecular Liquids*, vol. 307, p. 112921, Jun. 2020, ISSN: 0167-7322. DOI: [10.1016/j.molliq.2020.112921](https://doi.org/10.1016/j.molliq.2020.112921).
- [54] U. G. Būtaitė, G. M. Gibson, Y.-L. D. Ho, *et al.*, “Indirect optical trapping using light driven micro-rotors for reconfigurable hydrodynamic manipulation,” *Nature Communications*, vol. 10, no. 1, Mar. 2019, ISSN: 2041-1723. DOI: [10.1038/s41467-019-108968-7](https://doi.org/10.1038/s41467-019-108968-7).
- [55] Y. Tsuboi, T. Shoji, and N. Kitamura, “Optical trapping of amino acids in aqueous solutions,” *The Journal of Physical Chemistry C*, vol. 114, no. 12, pp. 5589–5593, Dec. 2009, ISSN: 1932-7455. DOI: [10.1021/jp9072334](https://doi.org/10.1021/jp9072334).
- [56] O. Y. Gowayed, T. Moosa, A. M. Moratos, *et al.*, “Dynamic light scattering study of a laser-induced phase-separated droplet of aqueous glycine,” vol. 125, pp. 7828–7839, 2021, ISSN: 1520-6106. DOI: [10.1021/acs.jpcb.1c02620](https://doi.org/10.1021/acs.jpcb.1c02620).
- [57] W. H. Orttung, “Polarizability and apparent radius of glycine from refractive index data,” *The Journal of Physical Chemistry*, vol. 67, no. 5, pp. 1102–1105, 1963, ISSN: 0022-3654. DOI: [10.1021/j100799a040](https://doi.org/10.1021/j100799a040).
- [58] E. J. Peterman, F. Gittes, and C. F. Schmidt, “Laser-induced heating in optical traps,” *Biophysical Journal*, vol. 84, no. 2, pp. 1308–1316, Feb. 2003, ISSN: 0006-3495. DOI: [10.1016/s0006-3495\(03\)74946-7](https://doi.org/10.1016/s0006-3495(03)74946-7).

## Bibliography

- [59] K.-i. Yuyama, T. Rungsimanon, T. Sugiyama, *et al.*, “Formation, dissolution, and transfer dynamics of a millimeter-scale thin liquid droplet in glycine solution by laser trapping,” *The Journal of Physical Chemistry C*, vol. 116, no. 12, pp. 6809–6816, Mar. 2012, ISSN: 1932-7455. DOI: 10.1021/jp210576k.